

Journal of Intelligent Material Systems and Structures

<http://jim.sagepub.com>

Toward Optimal Design of Piezoelectric Transducers Based on Multifunctional and Smoothly Graded Hybrid Material Systems

Wilfredo M. Rubio, Emilio C.N. Silva and Glaucio H. Paulino

Journal of Intelligent Material Systems and Structures 2009; 20; 1725 originally published online Jul 31, 2009;

DOI: 10.1177/1045389X09337085

The online version of this article can be found at:
<http://jim.sagepub.com/cgi/content/abstract/20/14/1725>

Published by:



<http://www.sagepublications.com>

Additional services and information for *Journal of Intelligent Material Systems and Structures* can be found at:

Email Alerts: <http://jim.sagepub.com/cgi/alerts>

Subscriptions: <http://jim.sagepub.com/subscriptions>

Reprints: <http://www.sagepub.com/journalsReprints.nav>

Permissions: <http://www.sagepub.co.uk/journalsPermissions.nav>

Citations <http://jim.sagepub.com/cgi/content/refs/20/14/1725>

Toward Optimal Design of Piezoelectric Transducers Based on Multifunctional and Smoothly Graded Hybrid Material Systems

WILFREDO M. RUBIO,^{1,*} EMILIO C. N. SILVA¹ AND GLAUCIO H. PAULINO²

¹*Department of Mechatronics and Mechanical Systems Engineering, Escola Politécnica da Universidade de São Paulo, Av. Prof. Mello Moraes, 2231 – Cidade Universitária, São Paulo – SP – 05508-900, Brazil*

²*Newmark Laboratory, Department of Civil and Environment Engineering University of Illinois at Urbana-Champaign, 205 North Mathews Av., Urbana, IL, 61801, USA*

ABSTRACT: This work explores the design of piezoelectric transducers based on functional material gradation, here named functionally graded piezoelectric transducer (FGPT). Depending on the applications, FGPTs must achieve several goals, which are essentially related to the transducer resonance frequency, vibration modes, and excitation strength at specific resonance frequencies. Several approaches can be used to achieve these goals; however, this work focuses on finding the optimal material gradation of FGPTs by means of topology optimization. Three objective functions are proposed: (i) to obtain the FGPT optimal material gradation for maximizing specified resonance frequencies; (ii) to design piezoelectric resonators, thus, the optimal material gradation is found for achieving desirable eigenvalues and eigenmodes; and (iii) to find the optimal material distribution of FGPTs, which maximizes specified excitation strength. To track the desirable vibration mode, a mode-tracking method utilizing the 'modal assurance criterion' is applied. The continuous change of piezoelectric, dielectric, and elastic properties is achieved by using the graded finite element concept. The optimization algorithm is constructed based on sequential linear programming, and the concept of continuum approximation of material distribution. To illustrate the method, 2D FGPTs are designed for each objective function. In addition, the FGPT performance is compared with the non-FGPT one.

Key Words: piezoelectric transducers, hybrid materials, functionally graded materials (FGMs), topology optimization, mode-tracking, continuum material distribution, mode assurance criterion (MAC), piezoelectric modal constant (PMC).

INTRODUCTION

PIEZOELECTRIC materials are multifunctional materials; they convert electrical energy (electric field and electric potential) into mechanical energy (stress and strain) and vice versa. Depending on the applications, there are different goals for designing piezoelectric transducers (Silva and Kikuchi, 1999), which are essentially related to the transducer resonance frequency, vibration modes, and excitation strength. In general, piezoelectric transducers with high excitation strength, at user-defined modes, are desired. Also, piezoelectric transducers oscillated at user-defined resonance frequencies and user-defined vibration mode shapes are desirable for resonator applications.

In the present work, an alternative approach is considered to achieve the above goals: to design piezoelectric transducers based on hybrid materials and functionally graded material (FGM) concepts. This class of materials includes those possessing continuously graded properties with gradual change in microstructure (Miyamoto et al., 1999). These materials are made to take advantage of desirable features of their constituent phases. For instance, in a thermal protection system, FGMs take advantage of heat and corrosion resistance, typical of ceramics; and mechanical strength and toughness, typical of metals. The piezoelectric transducer design, based on the FGM concept, is named functionally graded piezoelectric transducer (FGPT). It can be applied for improving transducer performance, such as local reduction of stress concentration (Wang and Noda, 2001) and stress redistribution, and increased bonding strength (and fatigue life) of bilaminar piezoelectric transducers (Qui et al., 2003). In addition, the FGM concept allows designing piezoelectric transducers

*Author to whom correspondence should be addressed.
E-mail: wilfredobw@usp.br, phone: 55-11-30915419
Figures 2, 3 and 7–18 appear in color online: <http://jim.sagepub.com>

with smaller time waveform (large bandwidth) (Guo et al., 2005; Rubio et al., 2009), which is desirable in medical imaging and non-destructive testing (NDT) applications. Essentially, either all FGPT properties (dielectric, elastic, and piezoelectric) or some of them vary along a specific direction, as shown in Figure 1.

Although, there exist literature concerning FGPT manufacturing, research that focuses on the systematic design and analysis of FGPT is rather scarce at present (Birman and Byrd, 2007). Most of the research related to modeling issues deals with applications of analytical and numerical techniques which, usually, grade a single material property of the FGPT; for instance, the elastic property c_{11} of a cantilever functionally graded piezoelectric beam subjected to normal load at the free end (Kruusing, 2000); or the piezoelectric property d_{31} (Hauke et al., 2000). The analytical modeling of graded piezoelectric actuators under bending, considering the simultaneous gradation along thickness of the piezoelectric property d_{31} and dielectric property ϵ_{33} , is discussed by Steinhausen et al. (2004). Other papers elucidating FGPT analytical modeling in free and forced vibrations include the ones by Yang and Xiang (2007), and Zhong and Yu (2006), and the nonlinear characteristics of functionally graded piezoelectric cantilever transducers under electromechanical loading (Shindo et al., 2009). On the other hand, for modeling 2D and 3D FGPTs or gradation of two or more properties using numerical techniques, a multilayer strategy is usually utilized, where at each lamina of the multilayer piezoceramic, the material properties are uniform, and change between layers. Almajid et al. (2001) and Taya et al. (2003) used a modified classic lamination theory (CLT) to evaluate the stress field and out-of-plane displacement of laminated piezoelectric transducers. They concluded that the gradation function changes

the FGPT performance, which suggests that optimization of the material property gradation function may lead to better transducer performance. Another multilayer approximation is the thin-layer method, which combines finite element method (FEM) with the spectral element method (Chakraborty et al., 2005), and the layer-wise laminate theory, developed for thermopiezoelectric beams, adapted to functionally graded piezoelectric bimorph beam analysis (Lee, 2005). Nevertheless, the accuracy of the multilayer approach is questionable for calculating stresses and simulating dynamic behavior because the stress concentration among layers is increased, and the numerical result depends on the number of layers utilized. In order to alleviate this problem, the material gradation is treated based on the graded finite element (GFE) concept (Santare and Lambros, 2000; Kim and Paulino, 2002). The GFE formulation incorporates the material property gradient at the size scale of the finite element, resulting in smooth change of properties among finite elements. Following that idea, Silva et al. (2007) extended the original structural GFE to quasi-static piezoelectric problems by using isoparametric finite elements. Other works extend the quasi-static GFE for structural dynamic modeling (Banks-Sills et al., 2002) and wave propagation modeling (Santare et al., 2003; Zhang and Paulino, 2007). In relation to optimized design of FGPTs, the work of Carbonari et al. (2007) shows that functionally graded bimorph-type piezoelectric quasi-static actuators based on the topology optimization method (TOM) and the GFE formulation can be achieved. In addition, the work of Carbonari et al. (2009) applies the TOM for finding the optimal gradation function of multi-actuated and flexensional piezoelectric actuators, considering quasi-static design. Nevertheless, the quasi-static design does not involve several important problems that arise in

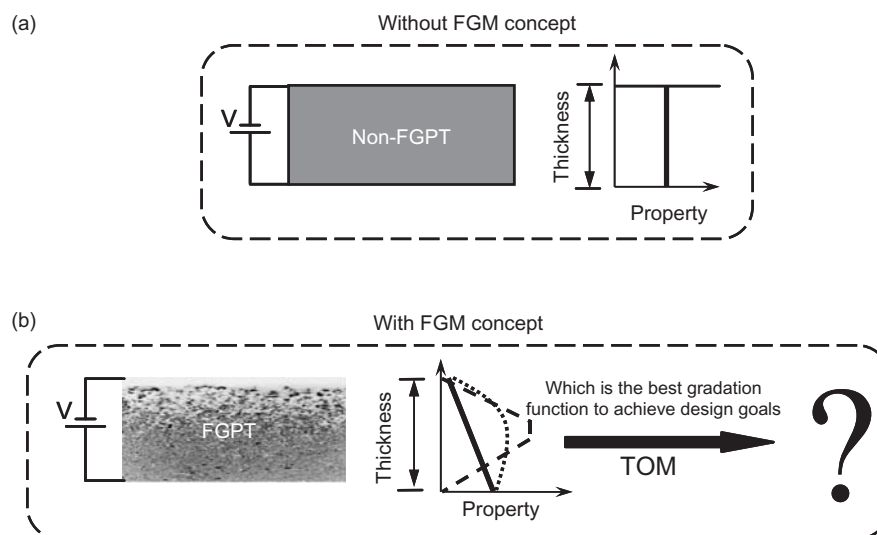


Figure 1. Piezoelectric transducer design principle: (a) without the FGM concept; (b) with the FGM concept, in conjunction with the topology optimization method, leading to a FGPT.

dynamic operations; such as non-smooth objective functions, eigenmode order switching in the optimization process, and discontinuous sensitivity of the objective function.

As mentioned above, several papers have shown that the gradation function can influence the performance of piezoelectric transducers (e.g., Almajid et al., 2001; Taya et al., 2003; Rubio et al., 2009); however, what is the best property gradation function for a specific dynamic application has not been demonstrated. Thus, in this work, TOM is applied to address this question. The TOM usually combines finite elements and optimization algorithms to maximize a design requirement. It has been applied to optimize a number of different mechanical and multiphysical systems (Bendsøe and Sigmund, 2003). In dynamic problems, a formulation using homogenization has been applied by Diaz and Kikuchi (1992) for eigenvalue optimization. Soto and Diaz (1993) considered optimal design of plate structures. They maximize higher order eigenvalues and also two eigenvalues simultaneously. Ma et al. (1995) used the same formulation to maximize the sum of a number of the lowest eigenvalues, aiming to reduce eigenmode order switching during the iterative optimization process. For piezoelectricity, TOM has been applied for designing piezocomposite materials (Silva et al., 1999; Sigmund and Torquato, 1999), piezoelectric actuators (Kögl and Silva, 2005) and microgrippers (Carbonari et al., 2005); piezoelectric resonators (Silva and Kikuchi, 1999; Ha and Cho, 2006), and graded piezoelectric actuators considering static analysis (Carbonari et al., 2007).

Usually, the topology optimized design of a structure consists of determining which points of space should be solid and which points should be void (i.e., no material); hence, a main question in topology optimization is how to change the material from zero (void) to one (material). A discrete material distribution function (0–1) would be very discontinuous resulting into difficulties in the numerical treatment of the problem due to multiple local minimum. Therefore, the problem must be relaxed by allowing the material to assume intermediate property values and, consequently, the geometric representation of the structure becomes similar to black-white (0–1) images together with some intermediate material regions or gray scale regions (Bendsøe and Sigmund, 2003). Generally, the intermediate material regions are removed in a post-processing state, which can produce, especially in dynamic design, dramatic reduction of optimal performance initially obtained by using the TOM. In this sense, a graded design, associated to gray scale (or intermediate material) of the topology optimization, arise as a more robust approach to design piezoelectric structures in dynamical analysis, and it may offer a better connection with manufacturing techniques (Carrillo-Heian et al., 2001).

In view of the above ideas, this research contributes: (i) to explore the TOM for designing FGPTs;

specifically, TOM is carried out in this investigation to modify, systematically, the dynamic characteristics of transducers; (ii) to extend the quasi-static piezoelectric GFE to piezoelectric eigenproblems; (iii) to develop a generic topology optimization formulation to find the optimum material gradation (Figure 1) in FGPTs in order to achieve specific goals: maximizing eigenvalues of user-defined vibration mode shapes, maximizing excitation strength of selective vibration mode shapes, and designing FGPTs with specified resonance frequencies and desired eigenmode shapes. Particularly, the FGPTs are required to oscillate in the piston-like mode, aiming at acoustic wave generation applications. To achieve these goals, a mode-tracking method is implemented to obtain the target eigenmode; specifically, the modal assurance criterion (MAC) is applied (Kim and Kim, 2000). To incorporate material gradation, the GFE formulation is implemented. The optimization algorithm is constructed based on sequential linear programming (SLP), and the concept of continuum approximation of material distribution (CAMD) (Matsui and Terada, 2004) for modeling a continuous distribution of material along the design domain. In addition, design variable projection (Guest et al., 2004; Almeida et al., 2008) is used to achieve an explicit material gradient control.

This article is organized as follows. In ‘Functionally Graded Piezoelectric Transducer Modeling’ section, the piezoelectric equilibrium and constitutive equations are shown. In ‘Tailored Topology Optimization Formulation’ section, the TOM is described, together with the three objective functions adopted. In ‘Numerical Implementation’ section, the numerical implementation and the sensitivity analysis are discussed. In ‘Results and Discussion’ section, 2D FGPTs are designed based on the objective functions defined in ‘Numerical Implementation’ section. To illustrate the features of the FGPT design, the performance of the designed FGPT is compared with the non-FGPT one. Finally, in ‘Summary and conclusions’ section, some conclusions are inferred.

FUNCTIONALLY GRADED PIEZOELECTRIC TRANSDUCER MODELING

Assuming the second-order strain tensor \mathbf{S} , and electrical field, \mathbf{E} , are independent variables, the constitutive piezoelectric equations are written (using Einstein’s convention) (Naillon et al., 1983):

$$\begin{aligned} T_{ij} &= C_{ijkl}^E(x, y)S_{kl} - e_{kij}(x, y)E_k \\ D_i &= e_{ikl}(x, y)S_{kl} + \varepsilon_{ik}^S(x, y)E_k \quad \text{for } i, j, k, l = 1, 2, 3 \end{aligned} \quad (1)$$

where \mathbf{T} and \mathbf{D} are the second-order stress tensor and the electric displacement, respectively. The elasticity tensor, \mathbf{C}^E (elastic stiffness at constant electric field), the

piezoelectric coefficient tensor, \mathbf{e} , and the dielectric constant tensor, $\boldsymbol{\varepsilon}^S$ (dielectric susceptibility at constant strain), are assumed to vary along the Cartesian coordinates x and y (for a bi-dimensional model). To complete the piezoelectric model, the mechanical and electrical equilibrium equations are applied. The mechanical balance corresponds to the calculation of the forces expressed by the Newton's equation and the electrical balance is expressed by Gauss' theorem (Naillon et al., 1983). After mathematical manipulation, the equilibrium balance equations for a piezoelectric medium are obtained as follows:

$$\begin{aligned} -\rho(x, y)\omega^2 u_i &= \frac{\partial}{\partial r_j} \left(C_{ijkl}^E(x, y) S_{kl} - e_{kij}(x, y) E_k \right) \\ \frac{\partial}{\partial r_j} (e_{ikl}(x, y) S_{kl} + \varepsilon_{ik}^S(x, y) E_k) &= 0 \end{aligned} \quad (2)$$

where ρ is the density of the material, which varies along the Cartesian coordinates x and y ; the term \mathbf{r} is a unit vector in the Cartesian coordinate system; the term \mathbf{u} is the displacement tensor; and ω is the circular frequency.

Finite Element Modeling

The matrix formulation of the equilibrium equations for a piezoelectric medium is given, without structural damping, as (Naillon et al., 1983; Lerch, 1990):

$$\begin{aligned} \begin{bmatrix} \mathbf{M}_{uu}(x, y) & 0 \\ 0 & 0 \end{bmatrix} \begin{Bmatrix} \ddot{\mathbf{U}} \\ \ddot{\boldsymbol{\varphi}} \end{Bmatrix} \\ + \begin{bmatrix} \mathbf{K}_{uu}(x, y) & \mathbf{K}_{u\varphi}(x, y) \\ \mathbf{K}_{\varphi u}(x, y) & \mathbf{K}_{\varphi\varphi}(x, y) \end{bmatrix} \begin{Bmatrix} \mathbf{U} \\ \boldsymbol{\varphi} \end{Bmatrix} &= \begin{Bmatrix} \mathbf{F} \\ \mathbf{Q} \end{Bmatrix} \end{aligned} \quad (3)$$

where \mathbf{U} is the nodal displacement vector; the term $\boldsymbol{\varphi}$ is the nodal electric potential vector; and \mathbf{F} and \mathbf{Q} are the nodal mechanical force and electric charge vectors, respectively. The terms \mathbf{M}_{uu} , \mathbf{K}_{uu} , $\mathbf{K}_{u\varphi}$, and $\mathbf{K}_{\varphi\varphi}$ are respectively the mass, elastic, piezoelectric, and dielectric matrices. However, when an FGPT is considered, the properties change continuously inside the piezoelectric domain, which means that the matrices of Equation (3) must be described by some continuous function of Cartesian position (x, y) into a bi-dimensional FGPT. Hence, the matrices of Equation (3) are expressed as:

$$\mathbf{M}_{uu}(x, y) = \iint \mathbf{N}_u^T \rho(x, y) \mathbf{N}_u \, dx \, dy \quad (4)$$

$$\mathbf{K}_{uu}(x, y) = \iint \mathbf{B}_u^T \mathbf{C}^E(x, y) \mathbf{B}_u \, dx \, dy \quad (5)$$

$$\mathbf{K}_{u\varphi}(x, y) = \iint \mathbf{B}_u^T \mathbf{e}^T(x, y) \mathbf{B}_\varphi \, dx \, dy \quad (6)$$

$$\mathbf{K}_{\varphi\varphi}(x, y) = - \iint \mathbf{B}_\varphi^T \boldsymbol{\varepsilon}^S(x, y) \mathbf{B}_\varphi \, dx \, dy \quad (7)$$

where \mathbf{N}_u are the shape functions for the displacements; and \mathbf{B}_u and \mathbf{B}_φ are the strain-displacement and voltage-gradient matrices, respectively; and the terms \mathbf{C}^E , \mathbf{e} , and $\boldsymbol{\varepsilon}^S$ represent the elastic, piezoelectric, and dielectric material properties, respectively. According to the theory of conventional finite elements, the matrices and vectors of piezoelectric constitutive equations result from assembling the vectors and matrices of single elements (Lerch, 1990).

In modal analysis, the eigenvalues and eigenmodes are found by solving the second-order system:

$$\begin{aligned} -\lambda \begin{bmatrix} \mathbf{M}_{uu}(x, y) & 0 \\ 0 & 0 \end{bmatrix} \begin{Bmatrix} \boldsymbol{\Psi}_u \\ \boldsymbol{\Psi}_\varphi \end{Bmatrix} \\ + \begin{bmatrix} \mathbf{K}_{uu}(x, y) & \mathbf{K}_{u\varphi}(x, y) \\ \mathbf{K}_{\varphi u}(x, y) & \mathbf{K}_{\varphi\varphi}(x, y) \end{bmatrix} \begin{Bmatrix} \boldsymbol{\Psi}_u \\ \boldsymbol{\Psi}_\varphi \end{Bmatrix} &= \begin{Bmatrix} 0 \\ 0 \end{Bmatrix} \end{aligned} \quad (8)$$

with $\lambda = \omega^2$

where λ and ω are the eigenvalue and natural frequency, respectively, and $\{\boldsymbol{\Psi}\} = \{\boldsymbol{\Psi}_u, \boldsymbol{\Psi}_\varphi\}^T$ represents the eigenmode vector.

Resonance and Antiresonance Frequencies

In piezoelectric structures, the electric impedance curve presents two extremes. The extremes correspond to resonance frequency (ω_r) or minimal electrical impedance condition, and antiresonance frequency (ω_a) or maximal electrical impedance condition (Naillon et al., 1983). The resonance and antiresonance frequencies are found by solving two problems with different boundary conditions in Equation (8): the resonance frequencies are found by exciting the FGPT with an electrical potential or simulating a short-circuit transducer, and the antiresonance frequencies are found by exciting the FGPT with electrical charges or simulating an open-circuit FGPT (Naillon et al., 1983).

Piezoelectric Modal Constant

The piezoelectric modal constant (PMC) determines, for a specific vibrating mode, how strong the coupling is between the mode and the excitation; in other words, the PMC determines the relative importance of a specific vibration mode. Accordingly, to increase the contribution of a specific mode, its PMC must be increased. The advantage of the PMC approach, in relation to the so called electromechanical coupling coefficient (widely used by calculating the excitation strength of a specific mode (Naillon et al., 1983; Lerch, 1990)), is that the PMC only requires knowledge of the resonance frequencies and, numerically, it can be easily evaluated, contrary to electromechanical coupling coefficient calculation, where several difficulties often arise to clearly identify both the resonance and antiresonance frequencies of a mode (Guo and Cawley, 1992).

The PMC (A_{r_k}) depends on the eigenmode Ψ_{r_k} of the resonance mode k , and it is formulated as (Guo and Cawley, 1992):

$$A_{r_k} = W_{r_k}^2 \quad (9)$$

with:

$$W_{r_k} = \{\Psi_{r_k}\}^T \{\mathbf{W}_F\} \quad (10)$$

where \mathbf{W}_F is the equivalent nodal force vector that converts the applied voltage on electrodes to a mechanical force at each finite element node. The equivalent nodal vector is given by (Guo and Cawley, 1992):

$$\{\mathbf{W}_F\} = \begin{bmatrix} \mathbf{K}_{u\varphi_p} \\ \mathbf{K}_{\varphi_o\varphi_p} \end{bmatrix} \{\mathbf{I}_p\} \quad (11)$$

where \mathbf{I}_p is a vector with length equal to the number of nodes on the electrode with varying potential (ungrounded electrode), and where the matrix $[\mathbf{K}_{u\varphi_p} \ \mathbf{K}_{\varphi_o\varphi_p}]^T$ results from transforming Equation (8) into a finite element equation where the nodes are grouped into electrode and non-electrode nodes (Naillon et al., 1983). Thus, for an FGPT excited by a voltage applied between a grounded electrode on its bottom surface and an ungrounded electrode on its top surface, Equation (8) becomes:

$$-\lambda \begin{bmatrix} \mathbf{M}_{uu} & 0 & 0 & 0 \\ 0 & 0 & 0 & 0 \\ 0 & 0 & 0 & 0 \\ 0 & 0 & 0 & 0 \end{bmatrix} \begin{Bmatrix} \Psi_u \\ \Psi_{\varphi_g} \\ \Psi_{\varphi_o} \\ \Psi_{\varphi_p} \end{Bmatrix} + \begin{bmatrix} \mathbf{K}_{uu} & \mathbf{K}_{u\varphi_g} & \mathbf{K}_{u\varphi_o} & \mathbf{K}_{u\varphi_p} \\ \mathbf{K}_{u\varphi_g}^T & \mathbf{K}_{\varphi_g\varphi_g} & \mathbf{K}_{\varphi_g\varphi_o} & \mathbf{K}_{\varphi_g\varphi_p} \\ \mathbf{K}_{u\varphi_o}^T & \mathbf{K}_{\varphi_o\varphi_g} & \mathbf{K}_{\varphi_o\varphi_o} & \mathbf{K}_{\varphi_o\varphi_p} \\ \mathbf{K}_{u\varphi_p}^T & \mathbf{K}_{\varphi_p\varphi_g} & \mathbf{K}_{\varphi_p\varphi_o} & \mathbf{K}_{\varphi_p\varphi_p} \end{bmatrix} \begin{Bmatrix} \Psi_u \\ \Psi_{\varphi_g} \\ \Psi_{\varphi_o} \\ \Psi_{\varphi_p} \end{Bmatrix} = \begin{Bmatrix} 0 \\ 0 \\ 0 \\ 0 \end{Bmatrix} \quad (12)$$

where the subscripts o , p , and g denote the electrical potential degree of freedom of the non-electrode nodes, ungrounded electrode nodes, and grounded electrode nodes, respectively. The sub-matrices $\mathbf{K}_{\varphi_p\varphi_p}$, $\mathbf{K}_{\varphi_g\varphi_g}$ and $\mathbf{K}_{\varphi_o\varphi_o}$ represent the dielectric stiffness matrices corresponding to nodes on the ungrounded electrode, nodes on the grounded electrode, and nodes which are not on one of the electrodes, respectively. The terms $\mathbf{K}_{u\varphi_p}$, $\mathbf{K}_{u\varphi_g}$, $\mathbf{K}_{u\varphi_o}$, $\mathbf{K}_{\varphi_o\varphi_p}$, $\mathbf{K}_{\varphi_o\varphi_g}$ and $\mathbf{K}_{\varphi_p\varphi_p}$ are corresponding coupling 'stiffness' matrices.

TAILORED TOPOLOGY OPTIMIZATION FORMULATION

This section addresses design requirements for piezoelectric transducers. Three objective functions are

implemented to demonstrate the validity and applicability of the proposed formulation and numerical techniques (FGM concept and TOM) for controlling and modifying the dynamic behavior of piezoelectric transducers in several applications (e.g., wave generations and resonators). Accordingly, these objective functions are essentially related to typical dynamic characteristics of piezoelectric transducers, such as the transducer resonance frequency, vibration modes, and the electromechanical coupling. The transducer design goals are given as:

- (i) to maximize the eigenvalue of specified vibration mode shapes;
- (ii) to target specified resonance frequencies (or eigenvalues) and specified mode shapes; and
- (iii) to maximize the excitation strength of specified eigenmodes.

These goals are addressed below.

Frequency Maximization

The present problem consists of finding the optimal material distribution of an FGPT, which maximizes the resonance frequency (or resonance eigenvalue) of a user-defined eigenmode. This problem is interesting because it is possible to emulate the operation of a piezoelectric transducer with reduced thickness. This fact makes FGPT manufacturing easier, especially, when an FGPT vibrates at a high fundamental frequency. The proposed multi-objective function is (Ma et al., 1995):

$$F_1 = \left(\frac{1}{\alpha} \sum_{k=1}^m w_k \lambda_{r_k}^{-1} \right)^{-1} \quad \text{with} \quad (13)$$

$$\alpha = \sum_{k=1}^m w_k; \lambda_{r_k} = \omega_{r_k}^2$$

where w_k are weight coefficients for mode k ($k = 1, 2, \dots, m$), the term m is the number of modes considered in the multi-objective function, and the parameters λ_{r_k} and ω_{r_k} are the resonance eigenvalue and resonance frequency for the mode k , respectively.

Transducer with Specified Resonance Frequencies

Here the goal is to design an FGPT that vibrates at desirable and user-defined resonance frequencies (or resonance eigenvalues) and eigenvectors; thus, the following requirements are necessary: (i) the specified resonance frequency (or resonance eigenvalue) must be achieved, and (ii) the FGPT is required to oscillate in a user-defined mode shape; for instance, the piston-like mode, aiming at acoustic wave generation applications. Hence, the multi-objective function is related to

target specified eigenvalues of user-defined eigenmodes (Ma et al., 1995; Silva and Kikuchi, 1999):

$$F_2 = - \left[\frac{1}{\alpha} \sum_{k=1}^m \frac{1}{\lambda_{0k}^2} (\lambda_{rk}^2 - \lambda_{0k}^2) \right]^{1/n} \quad \text{with} \quad (14)$$

$$\alpha = \sum_{k=1}^m \frac{1}{\lambda_{0k}^2}; \quad \lambda_{rk} = \omega_{rk}^2;$$

$$n = \pm 2, \pm 4, \pm 6, \pm 8, \dots$$

where λ_{rk} and λ_{0k} are the current resonance eigenvalue and user-specified eigenvalue for mode k ($k = 1, 2, \dots, m$), the term m is the number of modes considered in the multi-objective function, the constant n is a given power, and ω_{rk} is the corresponding resonance frequency for mode k ($k = 1, 2, \dots, m$). The objective function of Equation (14) allows piezoelectric resonator design with absence of spurious resonance frequencies close to the desirable one, or single-frequency FGPT.

PMC Maximization

The third multi-objective function consists of maximizing the PMC (A_r) of a specified mode or set of modes. As mentioned in ‘Piezoelectric Modal Constant’ section, the PMC is important because it evaluates how strong the excitation of a specific mode is in the transducer response. The multi-objective function is given by:

$$F_3 = \left[\frac{1}{\alpha} \left(\sum_{k=1}^m w_k A_{rk}^n \right) \right]^{1/n} \quad \text{with} \quad (15)$$

$$\alpha = \sum_{k=1}^m w_k;$$

$$n = -1, -3, -5, -7, \dots$$

where A_{rk} and w_k are respectively the PMC and weight coefficients for mode k ($k = 1, 2, \dots, m$), the term m is the number of modes considered, and n is a given power. The constant A_{rk} is defined in Equation (9).

Optimization Problem Formulation

This research explores the TOM for modifying the dynamic characteristics of FGPT by finding the optimal gradation function for that modification. Several goals can be implemented. Specifically, in this work, three objective functions are implemented F_j ($j = 1, 2, 3$), as mentioned in ‘Frequency Maximization’ ‘Transducer with Specified Resonance Frequencies’ and ‘PMC Maximization’. According to design requirements (defined above), the optimization problem can be formulated for finding the material gradation of an FGPT, in order to maximize any of the three multi-objective functions (F_1 , F_2 , or F_3) subjected to a piezoelectric volume constraint. That material constraint is implemented to control the piezoelectric material amount into the

design domain, Ω . In addition, the optimization method must target user-defined vibration mode shapes. Hence, the optimization problem is given as:

$$\begin{aligned} & \text{maximize} && F_j; \quad \text{for } j = 1, 2, \text{ or } 3 \\ & \rho_{\text{TOM}}(x, y) \\ & \text{subjected to:} && \int_{\Omega} \rho_{\text{TOM}}(x, y) d\Omega - \Omega_s \leq 0 \\ & && 0 \leq \rho_{\text{TOM}}(x, y) \leq 1 \\ & && \text{Equilibrium and Constitutive} \\ & && \text{Equation, see Equation (2)} \end{aligned} \quad (16)$$

where $\rho_{\text{TOM}}(x, y)$ is the design variable (or pseudo-density) at Cartesian coordinates x and y of a bi-dimensional FGPT, which does not necessarily represent the amount of material. The term Ω_s describes a constraint for ρ_{TOM} related to material type 1, at domain Ω ; see Equation (17).

The adopted material model is based on a simple extension of the traditional SIMP model (Bendsøe and Sigmund, 2003; Carbonari et al., 2007):

$$E^H(x, y) = \rho_{\text{TOM}}(x, y)E_1 + (1 - \rho_{\text{TOM}}(x, y))E_2 \quad (17)$$

where E^H denotes the ‘mixed’, homogenized, material properties. The term E_i is related to any elastic or piezoelectric or dielectric property for material type i ($i = 1, 2$). The parameter $\rho_{\text{TOM}} = 1.0$ denotes material properties type 1, and $\rho_{\text{TOM}} = 0.0$ denotes material properties type 2, which are referred with respect to Cartesian coordinates x and y of the bi-dimensional design domain Ω . Material type 1 and material type 2 refer to the fundamental material properties to be ‘mixed’ for setting up the FGPT properties (Carbonari et al., 2007).

Because FGPTs can be constructed by sintering a layer-structured green ceramic without any adhesive material, the optimization is arranged as a layer-like optimization problem; in other words, the design variables are considered equal at each layer, see Figure 2. This layer-like configuration makes the FGPT manufacturing possible. Although a layer-like optimization is implemented, the topology optimization problem maintains its continuous nature, as the GFE formulation (see ‘Numerical Implementation’ section) allows interpolating the materials properties inside each finite element; similarly, the design variables continuously change among finite elements, because they are defined at nodal level by using the CAMD formulation, see ‘Numerical Implementation’ section.

NUMERICAL IMPLEMENTATION

There are several relevant aspects in the numerical implementation of this work. A continuous material distribution is necessary along the bi-dimensional design

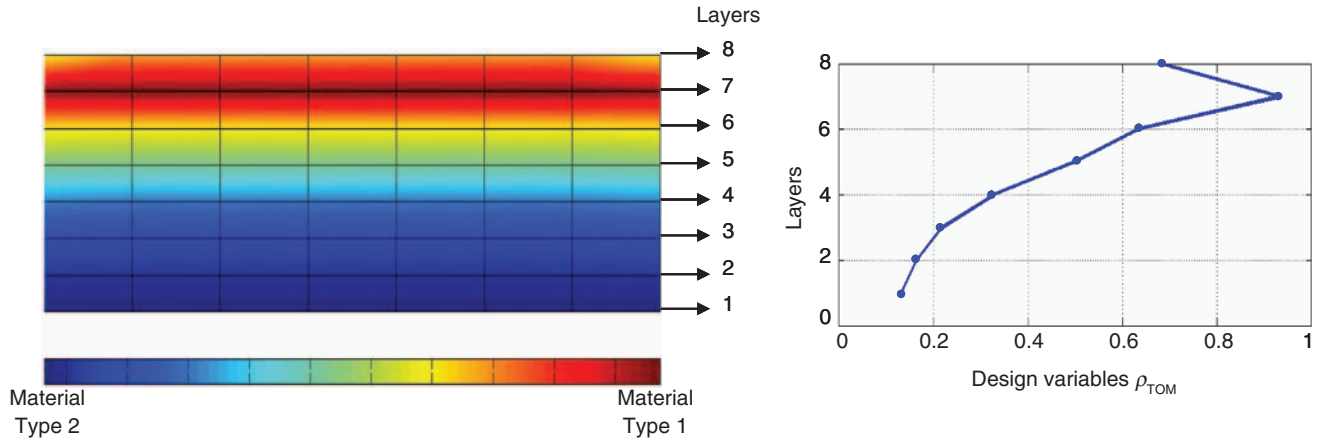


Figure 2. Layer-like design variables used in the optimization problem considering gradation along thickness direction.

domain Ω ; also, a continuous distribution of the design variables is necessary; in addition, the gradation functions found by using the TOM must be smooth; and finally, tracking a user-defined mode shape during the optimization process is required. To address these topics, the proposed formulation is based on four basic ideas: (i) the GFE formulation; (ii) the CAMD formulation; (iii) a modal-tracking strategy based on MAC; and (iv) a projection technique of the material distribution. Each implementation is explained below.

Graded Finite Element Applied to FGPT Design

Usually, in numerical implementations for dynamic applications, the FGPTs are simulated based on the traditional homogeneous finite element (HFE) or analytical approaches. In HFE the material properties are defined constants at the element level. The properties are evaluated at the centroid of each element. This approach is used in multilayer approaches (Almajid et al., 2001), which leads to undesirable discontinuities of the stress and strain fields (Kim and Paulino, 2002), and discontinuous material gradation. On the other hand, the analytical approaches are very constrained models; they are limited to 1D or single-property gradation models (Kruusing, 2000; Hauke et al., 2000). In this research, the generalized isoparametric formulation (GIF) by Kim and Paulino (2002) is extended to simulate FGPT in eigenvalue and eigenmode analysis. The eigenproblem for piezoelectricity (Equation (8)) is performed according to the technique by Yong and Cho (1996).

Contrary to multilayer approach, the GIF leads to a GFE where the material property gradient is continuously interpolated inside each finite element based on property values at each finite element node. The same shape functions N are used to interpolate unknowns (displacements and electrical potentials) and to interpolate the properties inside each finite element.

Hence, the density, ρ , and the elastic, C_{ijkl}^E , piezoelectric, e_{ikl} , and dielectric, ϵ_{ik}^S , material properties are respectively given by:

$$\begin{aligned} \rho(x, y) &= \sum_{n=1}^{n_d} N_n(x, y)\rho_n, \\ C_{ijkl}^E(x, y) &= \sum_{n=1}^{n_d} N_n(x, y)\left(C_{ijkl}^E\right)_n, \\ e_{ikl}(x, y) &= \sum_{n=1}^{n_d} N_n(x, y)(e_{ikl})_n, \\ \epsilon_{ik}^S(x, y) &= \sum_{n=1}^{n_d} N_n(x, y)(\epsilon_{ik}^S)_n \quad \text{for} \\ & \quad i, j, k, l = 1, 2, 3 \end{aligned} \tag{18}$$

where n_d is the number of nodes per finite element. When the GFE is implemented, the material properties must remain inside the integrals in Equations (4)–(7), and they must be properly integrated. On contrary, in HFE these properties usually are constants.

Continuous Approximation of Material Distribution

In traditional topology optimization formulations, the design variable is defined in a piecewise fashion in the discretized domain, which means that continuity of the material distribution is not realized between finite elements. However, considering the results of the topology optimization for an FGM-type material, a more natural way of representing the material distribution emerges by using the CAMD concept (Matsui and Terada, 2004; Rahmatalla and Swan, 2004), which essentially consists of finding a continuum optimum material distribution in the design domain. The CAMD considers that the design variables inside each finite element are interpolated by using, for instance, the finite element shape functions, N . Thus, the pseudo-density ρ_{TOM}^e at each graded finite element e can be expressed as:

$$\rho_{TOM}^e(x, y) = \sum_{i=1}^{n_d} \rho_{TOM_i}^n N_i(x, y) \tag{19}$$

where $\rho_{TOM_i}^n$ and N_i are the nodal design variable and shape function for node i ($i = 1, \dots, n_d$), respectively, and n_d is the number of nodes at each finite element. This formulation allows a continuous distribution of material along the design domain instead of the traditional piecewise material distribution applied by previous formulations of topology optimization (Bendsøe and Sigmund, 2003).

Projection of Material Distribution

The CAMD formulation is a useful tool for achieving continuous material distribution in the TOM; nevertheless, the CAMD does not provide a general control of the material distribution gradient. In this work, a scheme is implemented to achieve explicitly gradient control by introducing a layer of nodal variables on top of the existing nodal variables (Guest et al., 2004; Le, 2006; Almeida et al., 2008). The variables in the new layer are used as design variables, which are updated by the iterative optimization process.

The projection technique employs a function to relate the nodal design variable, $\rho_{TOM_i}^n$, to the nodal material density (pseudo-density), $\rho_{TOM_i}^p$. The projection function is defined as (Guest et al., 2004):

$$\rho_{TOM_i}^p = f(\rho_{TOM_i}^n) = \frac{\sum_{j \in S_i} \rho_{TOM_j}^n W(r_{ij})}{\sum_{j \in S_i} W(r_{ij})}$$

with $r_{ij} = \|\mathbf{x}_j - \mathbf{x}_i\|$ (20)

where $\rho_{TOM_j}^n$ is the design variable at node j ; the term $\rho_{TOM_i}^p$ is the material pseudo-density at node i ; and S_i is the set of nodes under influence of node i , see Figure 3. In other words, the sub-domain S_i corresponds to a circle with its center located at the node i and user-defined radius equal to r_{min} (Guest et al., 2004; Le, 2006) (Figure 3). The vectors \mathbf{x}_i and \mathbf{x}_j represent the Cartesian coordinates of node i and j , respectively. Moreover, the term W represents an appropriate weight function, which is given by:

$$W(r_{ij}) = \begin{cases} \frac{r_{min} - r_{ij}}{r_{min}} & \text{if } \mathbf{x}_j \in S_i \\ 0 & \text{otherwise} \end{cases} \quad (21)$$

However, other types of weight functions (e.g., quadratic or another non-linear function) can also be used, as explained by Almeida et al. (2008).

Discrete Optimization Problem

Considering a discretized domain by using GFE formulation, and the projection technique of the material

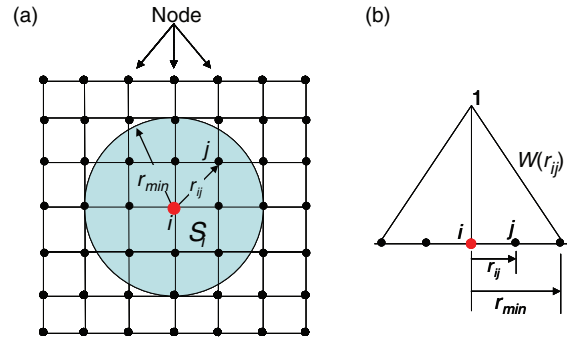


Figure 3. Projection technique: (a) definition of the length scale r_{min} ; (b) illustration of a linear projection function.

distribution, one obtains the implemented optimization problem, which is given by:

$$\begin{aligned} & \text{maximize} && F_j \quad \text{for } j = 1, 2, \text{ or } 3 \\ & \text{subjected to :} && \sum_{i=1}^{N_{type1}} \rho_{TOM_i}^n V_i - V^* \leq 0 \\ & && \text{for } i = 1 \dots N_{type1} \quad (22) \\ & && 0 \leq \rho_{TOM_i}^n \leq 1 \quad \text{for } i = 1 \dots N_{des} \\ & && \text{Equilibrium FE Equation,} \\ & && \text{see Equation (3)} \end{aligned}$$

where $\rho_{TOM_i}^n$ is the design variable of the node i ($i = 1, 2, \dots, N_{des}$). The parameter V_i is the material volume at node i ($i = 1, 2, \dots, N_{type1}$), and V^* describes a constraint for design variables $\rho_{TOM_i}^n$ related to material type 1. The terms N_{des} and N_{type1} denote the number of nodes of the discretized domain, and number of nodes with material type 1, respectively.

Mode-tracking Strategy

An important goal in this work is to maximize the objective functions of ‘Tailored Topology Optimization Formulation’ section and to target user-defined mode shapes. Thus, for example, in acoustic wave generations, such as non-destructive ultrasonic tests or ultrasonic medical image acquisitions, it is desirable that the piezoelectric transducer vibrates in the fundamental thickness extensional mode (also called the thickness dilatation mode or piston mode) to increase the amplitude of the emitted acoustic wave. In this work, the mode shape correlation coefficient (MSCC) or the MAC is implemented by tracking the desirable mode shape (Ewins, 1988).

The MAC has been widely used to compare experimental modal analysis with computational one (Ewins, 1988). However, in topology optimization, it was initially implemented to maximize eigenvalues associated with specified target modes of non-piezoelectric structures (Kim and Kim, 2000). Here, the MAC is utilized

to compare the user-defined or target mode shape, Ψ_{ref} , with the current eigenmode shape, Ψ_c , obtained from topology optimization process.

The MAC is defined as (Ewins, 1988):

$$MAC(\Psi_{ref}, \Psi_c) = \frac{|\Psi_{ref}^T \Psi_c|^2}{(\Psi_{ref}^T \Psi_{ref})(\Psi_c^T \Psi_c)} \quad (23)$$

The value of the MAC is a scalar quantity that varies between 0.0 and 1.0. When the MAC value is equal to 1.0, the vectors Ψ_{ref} and Ψ_c represent exactly the same eigenmode shape. However, it is difficult to provide precise values which the MAC should take in order to guarantee good results. In this work, a MAC value in excess of 0.9 represent highly correlated modes and a MAC value of less than 0.05 represent uncorrelated modes (Ewins, 1988).

Sensitivity Analysis

Usually, the sensitivities of objective functions (F_1 , F_2 , and F_3) and constraints with respect to design variables are required for topology optimization. Thus, the sensitivity calculation with respect to design variables ρ_{TOM}^n , based on sensitivities with respect to nodal pseudo-densities ρ_{TOM}^p , must be calculated.

Basically, any of the three objective functions, F , can be considered as a function of nodal pseudo-densities ρ_{TOM}^p , which are again a function of design variables ρ_{TOM}^n ; thus:

$$F \equiv F(\rho_{TOM}^p(\rho_{TOM}^n)) \quad (24)$$

where the variation (operator δ) of the function F is calculated as (considering the projection technique of ‘Projection of Material Distribution’ section) (Le, 2006):

$$\begin{aligned} &\delta F(\rho_{TOM}^p(\rho_{TOM_i}^n), \delta \rho_{TOM_i}^n, \delta \rho_{TOM_i}^n) \\ &= \sum_{k_n \in \Omega} \frac{\partial F}{\partial \rho_{TOM_{k_n}}^p} \delta \rho_{TOM_{k_n}}^p = \left(\sum_{j \in S_i} \frac{\partial F}{\partial \rho_{TOM_j}^p} \right) \delta \rho_{TOM_i}^n \end{aligned} \quad (25)$$

As the variation of $\rho_{TOM_i}^n$ causes the variation of a number of nodal pseudo-densities, which belong to the influence set S_i , see Figure 3, as follows:

$$\delta \rho_{TOM_j}^p(\rho_{TOM_i}^n, \delta \rho_{TOM_i}^n) = \begin{cases} \delta \rho_{TOM_i}^n & \text{for } j \in S_i \\ 0 & \text{otherwise} \end{cases} \quad (26)$$

where S_i corresponds to the circle with its center located at the node i and radius equal to r_{min} , according to projection technique. Hence, the sensitivity of objective function F , with respect to design variable $\rho_{TOM_i}^n$ of the

node i , is expressed as:

$$\frac{\partial F}{\partial \rho_{TOM_i}^n} = \sum_{j \in S_i} \frac{\partial F}{\partial \rho_{TOM_j}^p} \quad (27)$$

To complete the sensitivity analysis, the sensitivity calculation for each one of the objective functions, F equal to F_1 , F_2 , or F_3 , in relation to ρ_{TOM}^p is necessary. Each sensitivity is explained below (it is assumed that the design domain has been discretized by finite elements).

SENSITIVITY OF THE OBJECTIVE FUNCTION F_1

The sensitivity of the objective function F_1 can be obtained by deriving Equation (13) with relation to nodal pseudo-density $\rho_{TOM_j}^p$ of the node j and substituting this derivate at Equation (27). The gradient of F_1 with relation to $\rho_{TOM_j}^p$ is given as:

$$\frac{\partial F_1}{\partial \rho_{TOM_j}^p} = \left(\frac{1}{\alpha} \sum_{k=1}^m w_k \lambda_{r_k}^{-1} \right)^{-2} \sum_{k=1}^m \left(w_k \frac{1}{\lambda_{r_k}^{-2}} \frac{\partial \lambda_{r_k}}{\partial \rho_{TOM_j}^p} \right) \quad (28)$$

where $\partial \lambda_{r_k} / \partial \rho_{TOM_j}^p$ is the sensitivity of eigenvalue k with relation to the pseudo-density $\rho_{TOM_j}^p$. The sensitivity of the resonance eigenvalue is calculated by deriving the Equation (8) in relation to the pseudo-density $\rho_{TOM_j}^p$ following a procedure similar to that described by Haftka et al. (1990), and Silva and Kikuchi (1999). Hence, the following expression is obtained:

$$\begin{aligned} \frac{\partial \lambda_{r_k}}{\partial \rho_{TOM_j}^p} &= \begin{bmatrix} \Psi_u \\ \Psi_\varphi \end{bmatrix}_k^T \frac{\partial}{\partial \rho_{TOM_j}^p} \begin{bmatrix} \mathbf{K}_{uu}(x, y) & \mathbf{K}_{u\varphi}(x, y) \\ \mathbf{K}_{\varphi u}(x, y) & \mathbf{K}_{\varphi\varphi}(x, y) \end{bmatrix} \begin{bmatrix} \Psi_u \\ \Psi_\varphi \end{bmatrix}_k \\ &\quad - \lambda_{r_k} \begin{bmatrix} \Psi_u \\ \Psi_\varphi \end{bmatrix}_k^T \frac{\partial}{\partial \rho_{TOM_j}^p} \begin{bmatrix} \mathbf{M}_{uu}(x, y) & 0 \\ 0 & 0 \end{bmatrix} \begin{bmatrix} \Psi_u \\ \Psi_\varphi \end{bmatrix}_k \end{aligned} \quad (29)$$

and through Equation (4)–(7), the gradient of the mass and stiffness matrices is given as:

$$\begin{aligned} \frac{\partial}{\partial \rho_{TOM_j}^p} \mathbf{M}_{uu}(x, y) &= \sum_{e=1}^{Nel} \iint \mathbf{N}_u^T \frac{\partial \rho(x, y)}{\partial \rho_{TOM}^p} \frac{\partial \rho_{TOM}^p}{\partial \rho_{TOM_j}^p} \mathbf{N}_u \, dx \, dy \\ &= \sum_{e=1}^{nf} \iint \mathbf{N}_u^T \frac{\partial \rho(x, y)}{\partial \rho_{TOM}^p} N_j(x, y) \mathbf{N}_u \, dx \, dy \end{aligned} \quad (30)$$

$$\begin{aligned} \frac{\partial}{\partial \rho_{TOM_j}^p} \mathbf{K}_{uu}(x, y) &= \sum_{e=1}^{Nel} \iint \mathbf{B}_u^T \frac{\partial C^E(x, y)}{\partial \rho_{TOM}^p} \frac{\partial \rho_{TOM}^p}{\partial \rho_{TOM_j}^p} \mathbf{B}_u \, dx \, dy \\ &= \sum_{e=1}^{nf} \iint \mathbf{B}_u^T \frac{\partial C^E(x, y)}{\partial \rho_{TOM}^p} N_j(x, y) \mathbf{B}_u \, dx \, dy \end{aligned} \quad (31)$$

$$\frac{\partial}{\partial \rho_{\text{TOM}_j}^p} \mathbf{K}_{u\varphi}(x, y) = \sum_{e=1}^{nf} \iint \mathbf{B}_u^T \frac{\partial \mathbf{e}^T(x, y)}{\partial \rho_{\text{TOM}}^p} N_j(x, y) \mathbf{B}_\varphi \, dx \, dy \tag{32}$$

$$\frac{\partial}{\partial \rho_{\text{TOM}_j}^p} \mathbf{K}_{\varphi\varphi}(x, y) = - \sum_{e=1}^{nf} \iint \mathbf{B}_\varphi^T \frac{\partial \mathbf{e}^S(x, y)}{\partial \rho_{\text{TOM}}^p} N_j(x, y) \mathbf{B}_\varphi \, dx \, dy \tag{33}$$

where the parameter Nel is the total number of finite elements, and nf is the number of elements connected at node j ; in other words, the summation of the gradient of the mass and stiffness matrices ($\partial \mathbf{M}_{uu} / \partial \rho_{\text{TOM}_j}^p$, $\partial \mathbf{K}_{uu} / \partial \rho_{\text{TOM}_j}^p$, $\partial \mathbf{K}_{u\varphi} / \partial \rho_{\text{TOM}_j}^p$, and $\partial \mathbf{K}_{\varphi\varphi} / \partial \rho_{\text{TOM}_j}^p$) is performed considering only those elements connected at node j . The gradient of the material properties (elastic, piezo-electric, and dielectric) and density are straightforward and are obtained by differentiating Equation (18), and by considering the material model of Equation (17).

SENSITIVITY OF THE OBJECTIVE FUNCTION F_2

The sensitivity of objective function F_2 can be obtained by differentiating Equation (14); hence, that gradient is given as:

$$\frac{\partial F_2}{\partial \rho_{\text{TOM}_j}^p} = -F_2^{(1-n)} \sum_{k=1}^m \frac{1}{\lambda_{0k}^2} \frac{1}{(\lambda_{rk} - \lambda_{0k})^{1-n}} \frac{\partial \lambda_{rk}}{\partial \rho_{\text{TOM}_j}^p} \tag{34}$$

where the term $\partial \lambda_{rk} / \partial \rho_{\text{TOM}_j}^p$ is expressed in Equation (29). To find the sensitivity of F_2 with relation to design variables $\rho_{\text{TOM}_j}^p$, it is necessary to substitute Equation (34) into Equation (27).

SENSITIVITY OF THE OBJECTIVE FUNCTION F_3

The sensitivity of objective function F_3 with relation to pseudo-densities $\rho_{\text{TOM}_j}^p$ can be expressed as (differentiating the Equation (15) with relation to $\rho_{\text{TOM}_j}^p$):

$$\frac{\partial F_3}{\partial \rho_{\text{TOM}_j}^p} = -F_3^{(1-n)} \sum_{k=1}^m w_k \frac{1}{A_{rk}^{1-n}} \frac{\partial A_{rk}}{\partial \rho_{\text{TOM}_j}^p} \tag{35}$$

To complete the sensitivity of the objective function F_3 , the gradient of PMC of the mode k ($\partial A_{rk} / \partial \rho_{\text{TOM}_j}^p$), with relation to pseudo-density $\rho_{\text{TOM}_j}^p$ of node j , is required. This gradient is obtained by differentiating Equation (9); thus:

$$\begin{aligned} \frac{\partial A_{rk}}{\partial \rho_{\text{TOM}_j}^p} = & 2W_{rk} \left(\frac{\partial \{\Psi_{rk}\}^T}{\partial \rho_{\text{TOM}_j}^p} \begin{bmatrix} \mathbf{K}_{u\varphi_p} \\ \mathbf{K}_{\varphi_o\varphi_p} \end{bmatrix} \right. \\ & \left. + \{\Psi_{rk}\}^T \frac{\partial}{\partial \rho_{\text{TOM}_j}^p} \begin{bmatrix} \mathbf{K}_{u\varphi_p} \\ \mathbf{K}_{\varphi_o\varphi_p} \end{bmatrix} \right) \{\mathbf{I}_p\} \tag{36} \end{aligned}$$

The sensitivity of the k -th eigenmode Ψ_{rk} , in resonance, with respect to the j -th pseudo-density $\rho_{\text{TOM}_j}^p$, is calculated based on Wang’s approach (Sutter et al. 1988; Wang, 1990). The basic idea includes using the modal technique that represents the sensitivity of eigenmodes as a linear combination of eigenmodes themselves. That is, the eigenmode sensitivity is obtained as follows:

$$\frac{\partial \{\Psi_{rk}\}}{\partial \rho_{\text{TOM}_j}^p} = \sum_{c=1}^{N_{\text{mode}}} a_{ijk} \{\Psi_{rc}\} \tag{37}$$

where:

$$a_{ijk} = \frac{\{\Psi_{rc}\}^T \begin{pmatrix} \partial / \partial \rho_{\text{TOM}_j}^p \begin{bmatrix} \mathbf{K}_{uu}(x, y) & \mathbf{K}_{u\varphi}(x, y) \\ \mathbf{K}_{u\varphi}(x, y) & \mathbf{K}_{\varphi\varphi}(x, y) \end{bmatrix} \\ -\lambda_{rk} \left(\partial / \partial \rho_{\text{TOM}_j}^p \right) \begin{bmatrix} \mathbf{M}_{uu}(x, y) & 0 \\ 0 & 0 \end{bmatrix} \end{pmatrix} \{\Psi_{rk}\}}{\lambda_{rk} - \lambda_{rc}} \tag{38}$$

for $c \neq k$

and

$$a_{ijk} = -\frac{1}{2} \{\Psi_{rk}\}^T \frac{\partial}{\partial \rho_{\text{TOM}_j}^p} \begin{bmatrix} \mathbf{M}_{uu}(x, y) & 0 \\ 0 & 0 \end{bmatrix} \{\Psi_{rk}\} \tag{39}$$

for $c = k$

and N_{mode} is an appropriate number of the eigenmodes associated with the lowest eigenvalues (Sutter et al., 1988; Wang, 1990).

Optimization Procedure

Figure 4 shows a flow chart of the optimization algorithm. Initially, the initial domain is discretized by graded finite elements and the design variables are defined at each node. The initial guess for design variables ρ_{TOM}^p is chosen to be the same as the initial guess for material density at nodes, ρ_{TOM}^p .

The Q4/Q4 finite element is used (Rahmatalla and Swan, 2004), see Figure 5, which represents a 2D four-node quadrilateral FE, each node with three degrees of freedom: two mechanics (horizontal and vertical displacements), and one electric (electrical potential); in addition, each node has a design variable. A fully isoparametric formulation is developed in the sense that the same bilinear shape functions are applied to interpolate the unknown displacements and electric potentials, the geometry, and the material properties. In this work, the SLP is applied to solve the non-linear optimization problem of Equation (16) (Haftka et al., 1990). It consists of the sequential solution of approximated linear

sub-problems that can be defined by writing a Taylor series expansion for the non-linear optimization problem, around the current design point ρ_{TOM}^n at each iteration step. This linearization requires the sensitivities (gradients) of the objective function and constraints in relation to ρ_{TOM}^n and ρ_{TOM}^p . The sensitivity calculation is given in ‘Sensitivity Analysis’ section.

By using the MAC values, the objective eigenvectors are selected first, and then the sensitivity analysis is carried on those selected eigenvectors. Accordingly, at each iteration, the MAC values are calculated by comparing, see Equation (23), the user-defined target or reference mode shapes with those obtained by solving the eigenproblem of Equation (8). Then, the eigenvectors having the MAC value closest to 1 are selected as the objective eigenmode shapes. When the current shapes substantially change during the optimization process, the reference eigenmode shapes are updated.

In addition, at each iteration, moving limits are defined for the design variables ρ_{TOM}^n . Typically, during the iterative process, the design variables will be allowed to change by 5–15% of the original values. After linear optimization, a new set of design variables ρ_{TOM}^n and material pseudo-density ρ_{TOM}^p are obtained and updated

in the design domain until convergence is achieved for the objective function. The procedure converges when the changes in design variables from iteration to iteration are below 10^{-3} . The final material distribution is found by projecting the design variables onto material pseudo-density layer. The finite element analysis used to obtain the response fields (electrical potentials and displacements) is based on this projected material distribution.

RESULTS AND DISCUSSION

To illustrate the proposed method, 2D FGPTs are designed considering plane strain assumption.

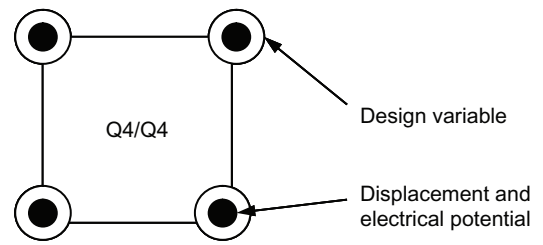


Figure 5. The Q4/Q4 finite element.

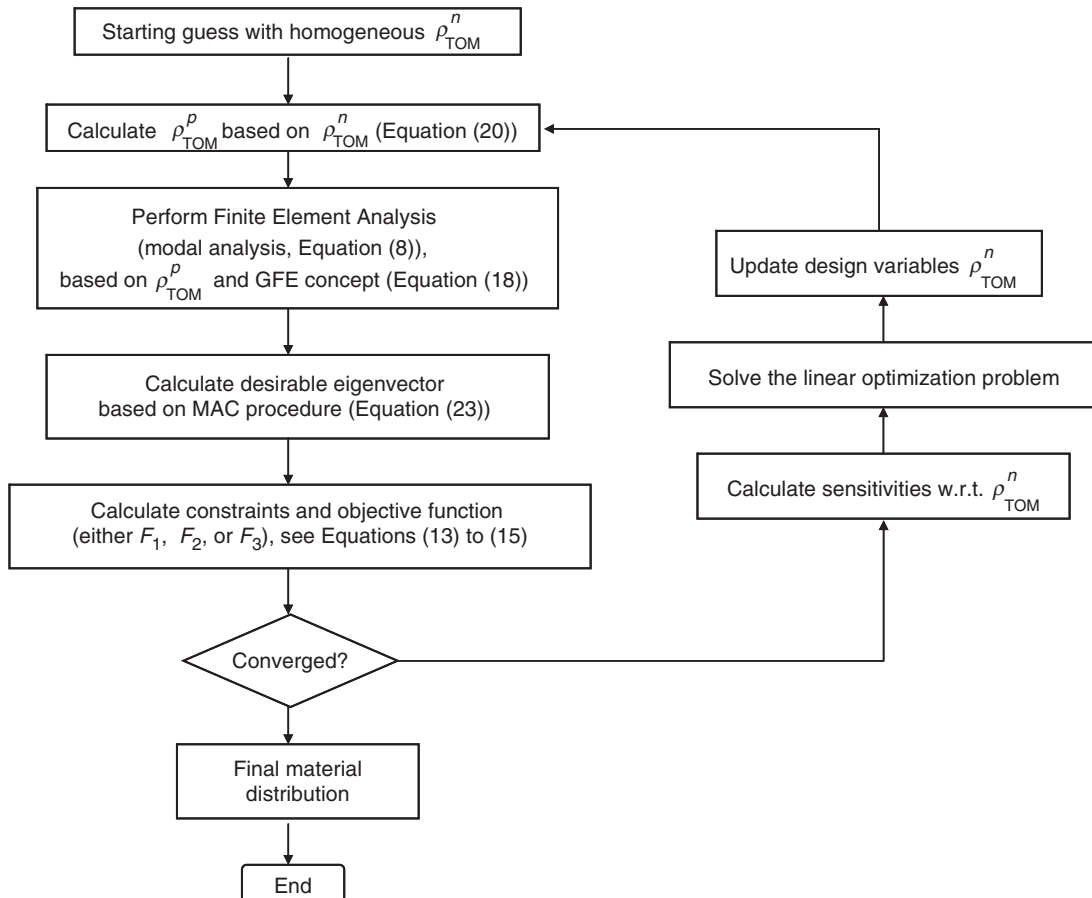


Figure 4. Flow chart of the optimization procedure.

The results are divided into three sets. The first set shows the results when the resonance frequency of a user-defined eigenmode is increased. The second set deals with achieving specified eigenvalues and vibration mode shapes. Finally, the third set consists of maximizing the PMC of a specified mode shape. The design domain used is shown in Figure 6. It is specified as a 20 mm by 5 mm rectangle with two fixed support at the ends (left- and right-hand side). The idea is to distribute simultaneously two types of materials into the design domain. In all cases, the material type 1 is PZT-5A piezoelectric ceramic. As material type 2, piezoelectric and non-piezoelectric materials can be used. Table 1 shows all material properties used. For all results, the design domain contains initially PZT-5A material.

PZT-5A Dynamic Characterization

Before addressing FGPTs (using the FGM concept), a brief description of dynamic behavior of PZT-5A ceramics (material type 1) is given. The design domain is shown in Figure 6, and the PZT-5A properties are given in Table 1. A finite element discretization of 50 × 30 finite elements is used. The mesh was chosen as a compromise between accuracy and efficiency. Hence, an FE convergence analysis is performed for finding the adequate mesh for simulations. Figure 7 shows the FE convergence curve. The design domain of Figure 6 is discretized into 400 (20 × 20), 900 (30 × 30), 1200 (40 × 30), 1500 (50 × 30), 2400

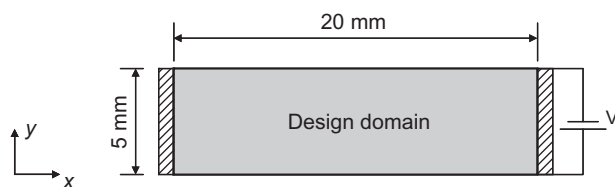


Figure 6. Design domain for optimal FGPT. The length is 20mm and the thickness is 5mm.

(60 × 40), 3500 (70 × 50), and 5600 (80 × 70) finite elements without considering gradation effects. The convergence on frequency value of the piston-like mode is reached using 1500 (50 × 30) finite elements. Additional increments in mesh size are accompanied by high increases in computational time, and the improvements in computational accuracy on frequency value are deemed sufficiently small. For instance, if the mesh is incremented to 5600 FE, the frequency accuracy of the piston-like mode is only incremented by 0.1%. Additionally, the mesh density is chosen so there are enough finite element nodes per wavelength of the highest mode required. In this case, as the highest frequency required is 1 MHz, the PZT-5A wavelength is 4.39 mm; hence, with a 50 × 30 mesh, there are always 11 and 27 nodes per wavelength on thickness (y direction in Figure 6) and longitudinal (x direction in Figure 6) directions, respectively. The simulations do not take any PZT-5A material loss into account.

Figure 8 shows the types of vibration modes predicted by FEA, considering the design domain of Figure 6,

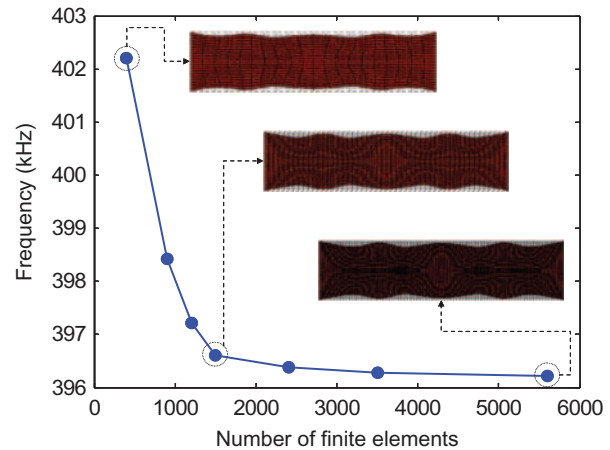


Figure 7. Convergence history of the FE mesh for piston-like mode. The design domain of Figure 6 is discretized with (400, 900, 1200, 1500, 2400, 3500, 5600) FEs.

Table 1. Material properties (Kino, 2000).

Properties		PZT-5A	PZT-2	PZT-5H	Epoxy polymer
Dielectric properties (F/m)	ϵ_0	8.85×10^{-12}	8.85×10^{-12}	8.85×10^{-12}	8.85×10^{-12}
	ϵ_{11}^S	$916 \times \epsilon_0$	$504 \times \epsilon_0$	$1700 \times \epsilon_0$	$3.6 \times \epsilon_0$
	ϵ_{33}^S	$830 \times \epsilon_0$	$260 \times \epsilon_0$	$1470 \times \epsilon_0$	$3.6 \times \epsilon_0$
Piezoelectric properties (C/m ²)	e_{31}	-5.4	-109	-6.5	0.0
	e_{33}	15.8	9.0	23.30	0.0
	e_{15}	12.3	9.8	17.0	0.0
	Elastic properties (N/m ²)	C_{11}^E	12.1×10^{10}	13.5×10^{10}	12.6×10^{10}
C_{12}^E		7.54×10^{10}	7.54×10^{10}	7.59×10^{10}	9.34×10^9
C_{13}^E		7.52×10^{10}	7.52×10^{10}	8.41×10^{10}	9.34×10^9
C_{33}^E		11.1×10^{10}	11.3×10^{10}	11.7×10^{10}	9.34×10^9
C_{44}^E		2.11×10^{10}	2.11×10^{10}	2.30×10^{10}	9.34×10^9
C_{66}^E		2.28×10^{10}	2.28×10^{10}	2.50×10^{10}	9.34×10^9
Density (kg/m ³)		7500	7500	7500	1340

and the material properties of Table 1 (PZT-5A properties). Also, Figure 8 shows for each mode the respective resonance frequency and the order number considering both elastic and piezoelectric modes (in parentheses).

From Figure 8 two vibrational modes can be identified, according to the classification by Guo and Cawley (1992): the thickness shear modes (TS modes) and thickness extensional modes (TE modes). The radial modes (R modes) and edge modes (E modes) are not present as the used boundary conditions (Figure 6) remove them. With TS modes the axial mean value (vertical displacement) is zero and with TE modes the axial mean value is non-zero; hence, usually TE modes are the most interesting and important modes for piezoelectric applications. It is observed that the piezoelectric mode 5 (or mode 23, including elastic and piezoelectric modes) is similar to piston-like mode of 1D

piezoelectric modes. In addition, mode number 5 (23) has the highest PMC, see Figure 9(a). This PMC quantifies the excitation strength of a specific mode; in other words, mode number 5 (23) is the strongest mode excited by any applied voltage.

Finally, Figure 9(b) shows the corresponding mechanical frequency response function (FRF), with a resolution of 0.5 kHz, in which the response is the axial mechanical displacement at the central point on the top surface of the piezoceramic when it is excited with an input voltage equal to 100 V. Notice that spikes appear at the resonance frequency, which confirms the frequency values per mode shown in Figure 8. All the 12 piezoelectric modes shown in Figure 8 are present in Figure 9(b), although some of them are too weak to be distinguished. Moreover, in the present article, displacement rather than electrical impedance is used to illustrate the FRF. This has been done because the

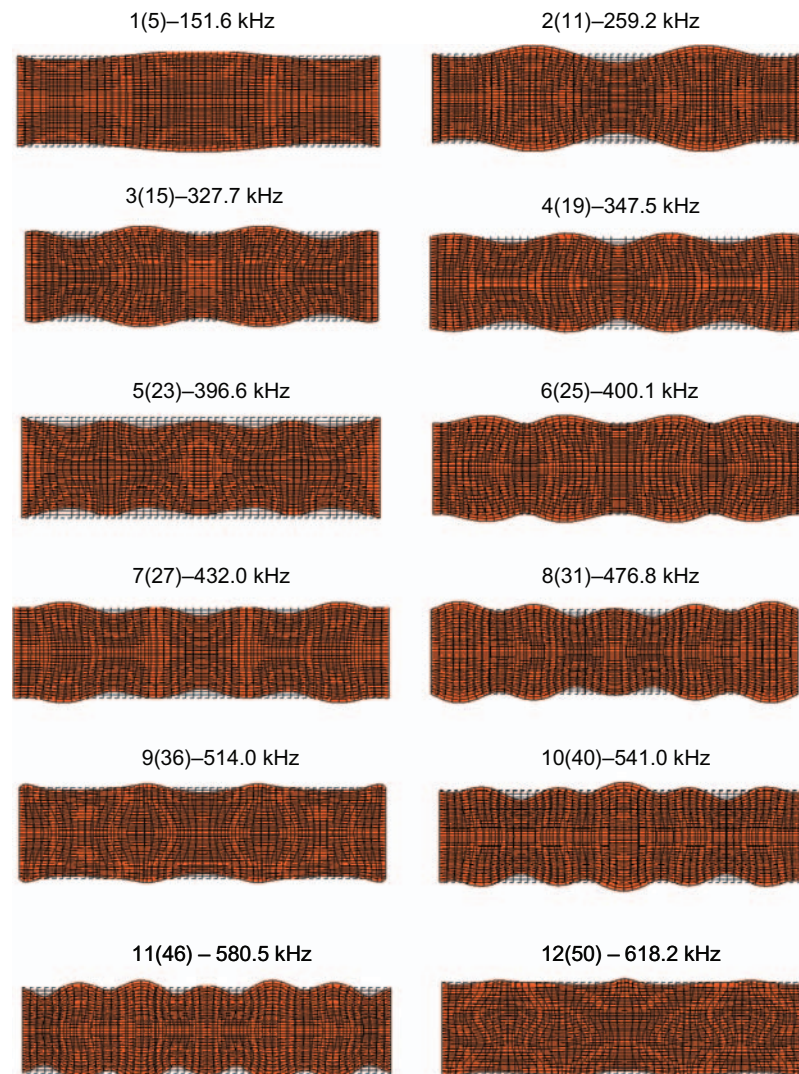


Figure 8. Vibrational mode types predicted by FEA (PZT-5A). The notation # (#) – # kHz means: first number, mode number considering only piezoelectric modes; second number (in parentheses), mode number considering all modes (elastic and piezoelectric); third number, resonance frequency (kHz).

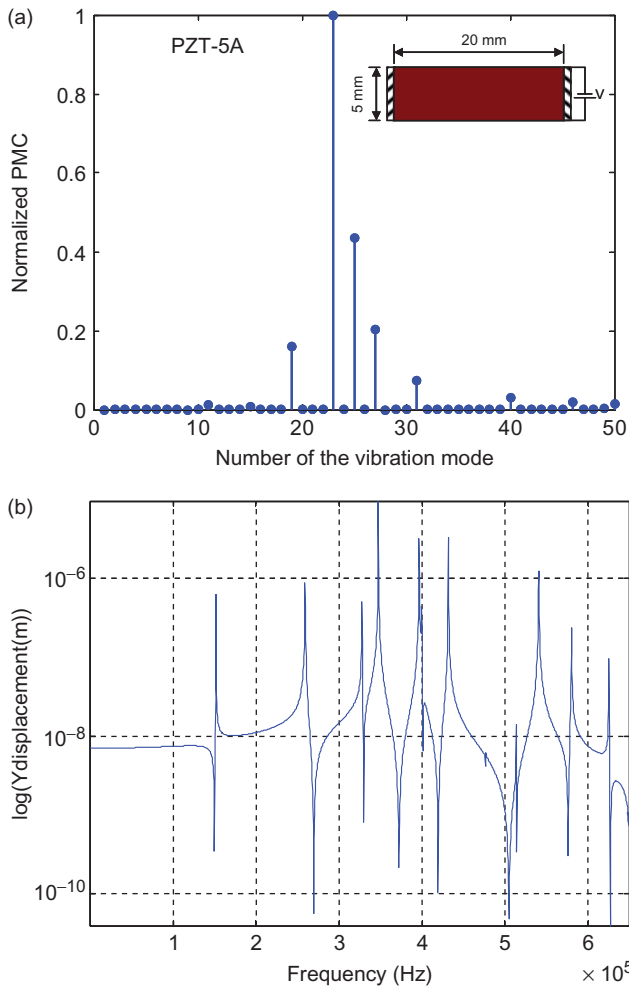


Figure 9. Piezoelectric transducer (PZT-5A): (a) PMC and (b) axial mechanical FRF at the central point of the top surface (Figure 6).

resonance peaks are clearer in the displacement plots than in the impedance plots.

Eigenvalue Maximization of User-defined Mode Shape

In this section, an FGPT with maximized selective eigenvalues is designed; in other words, the objective function F_1 is maximized. The material type 2 is considered as a non-piezoelectric material; thus, an FGPT type piezoelectric/non-piezoelectric is designed. An epoxy polymer is used as material type 2, with properties given by Table 1. In this work, the materials are chosen for demonstrating the capability of FGM concept, together with TOM, to modify the dynamics of piezoelectric transducers, and it may not represent the actual material distribution within an actual FGPT as it will be subjected to other fabrication constraints. A mesh discretization of 50×30 finite elements is utilized. Other parameters adopted in optimization are shown in Table 2. The target eigenmode is defined as the

Table 2. Parameters used in TOM.

Data	Value
Number of smallest eigenvalues to be computed in FE analysis	60
Volume constraint of PZT-5A material	80%
Initial guess for design variables	1, which is equivalent to material type 1 (PZT-5A)

piezoelectric mode number 5 (or mode number 23 considering elastic modes), which vibrates at piston-like mode, as shown in Figure 8 for the PZT-5A. Moreover, gradation along thickness is assumed.

Figure 10 shows the convergence history curves for eigenvalue, mode position during the optimization process, and MAC value, considering the projection technique. The curves of multi-objective function and eigenvalue convergence are the same curve (Figure 10(a)), since m is equal to 1 in Equation (13). An increase of 112% is achieved, as FGPT concept allows increasing the initial eigenvalue from $6.20 \times 10^{12} \text{ Hz}^2$ (corresponding to PZT-5A material) to $13.16 \times 10^{12} \text{ Hz}^2$ (corresponding to FGPT). However, it is observed in Figure 10 that their orders during the optimization process, which results in a non-smooth curve. This is evident in Figure 10(b), where it is noticed that the initial mode (mode number 23 including elastic modes) moves to mode number 29 at iteration 10, then it moves to mode number 12 at iteration 12, then to mode number 34 at iteration 14, and finally, it stabilizes at mode number 35. To turn the objective function into a smooth curve, it is necessary to use an m value different from 1 in Equation (13); maximizing a mean-eigenvalue (Ma et al., 1995), which probably contains the contribution of all modes. However, this approach is not useful due to high computational cost when a high order mode is optimized, as in this example, where the initial mode number 23 is maximized.

On the other hand, Figure 10(c) shows that MAC value change from 1 to 0.41; however, this value (0.41) represents a good correlation between initial user-defined eigenmode and achieved eigenmode. This fact is corroborated in Figure 11, where it is observed that the final mode shape (mode 35) is very close to the initial mode shape (mode 23), compare Figure 11(a) and Figure 11(b), respectively. Accordingly, the final topology is a thickness extensional mode, which generates a mean axial displacement higher than zero on the top and bottom surfaces. In addition, the final mode shape vibrates like piston mode. Also, Figure 11(c) exhibits the final material distribution function. This function depicts an FGPT with material PZT-5A in the middle and epoxy polymer-rich region on the top and bottom surfaces. In this example, the projection technique

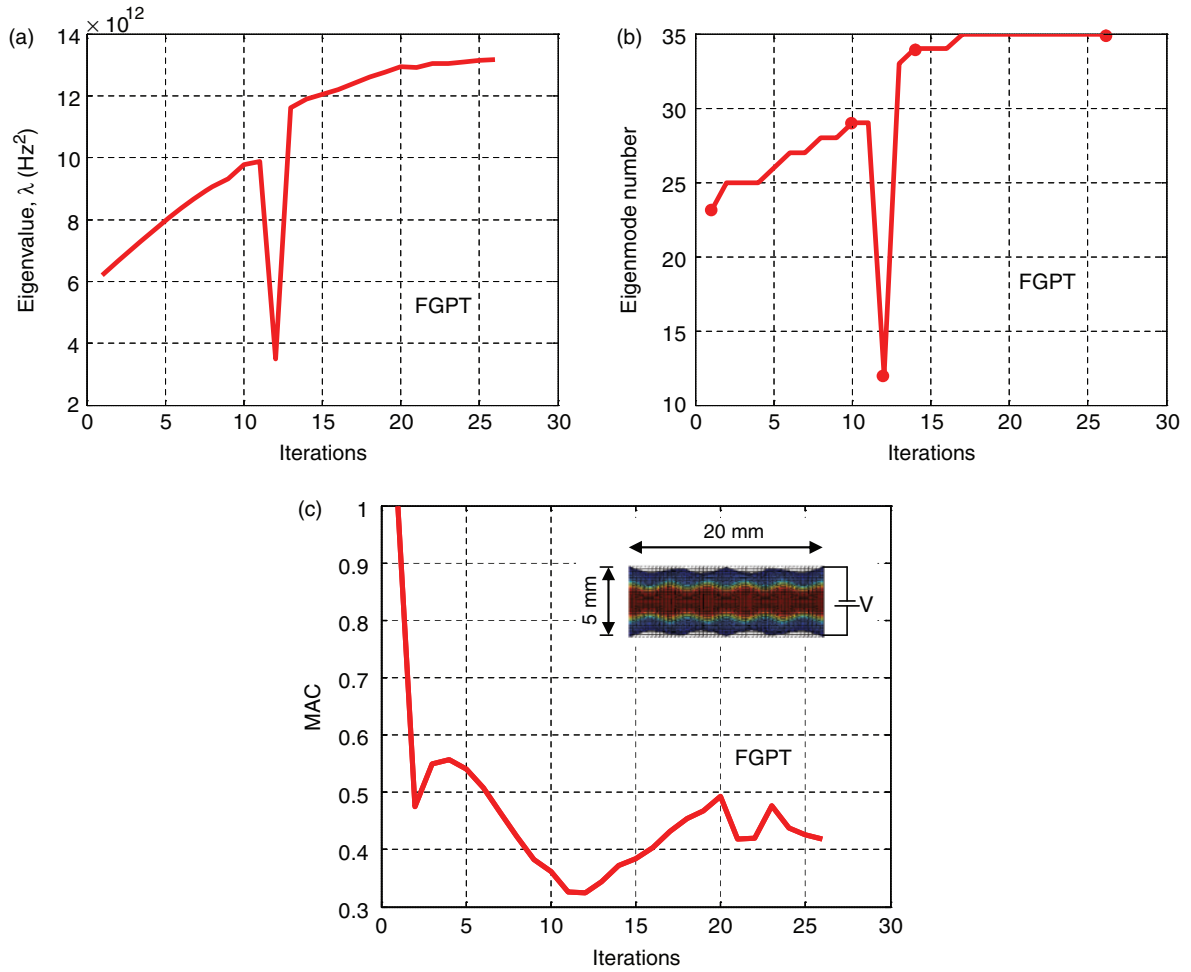


Figure 10. Convergence history curves for FGPT: (a) eigenvalue, (d) mode position and (b) MAC value.

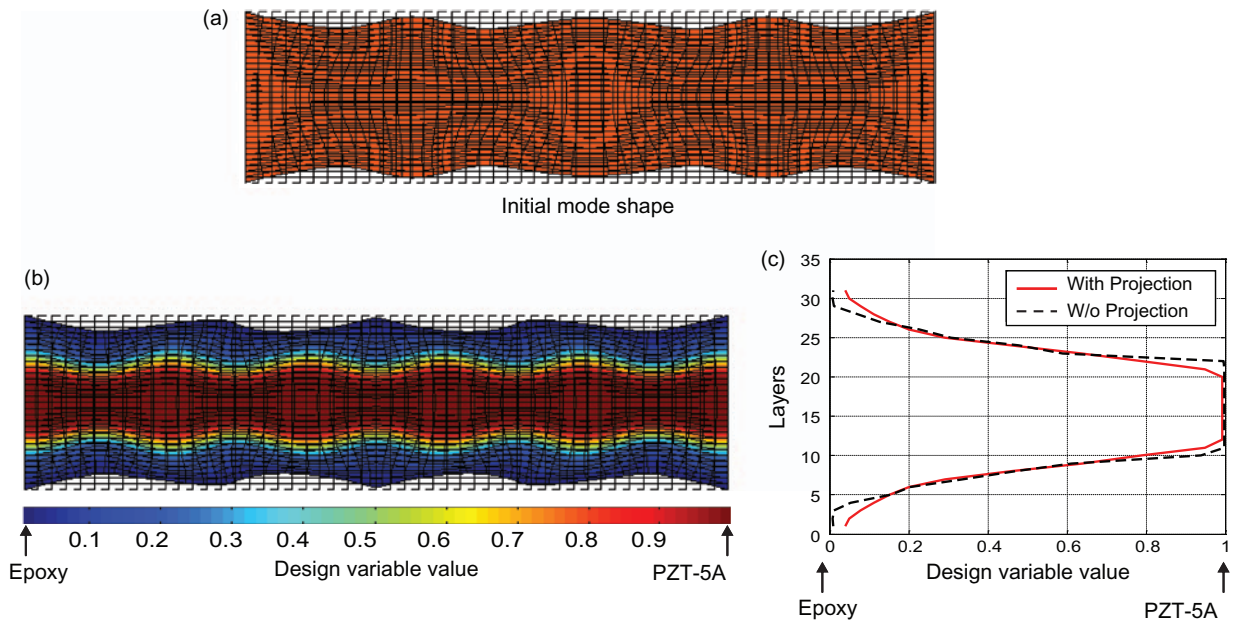


Figure 11. FGPT: (a) Initial mode shape (dashed and solid line respectively depict non-deformed and deformed structure); (b) final mode shape; (c) final material distribution function.

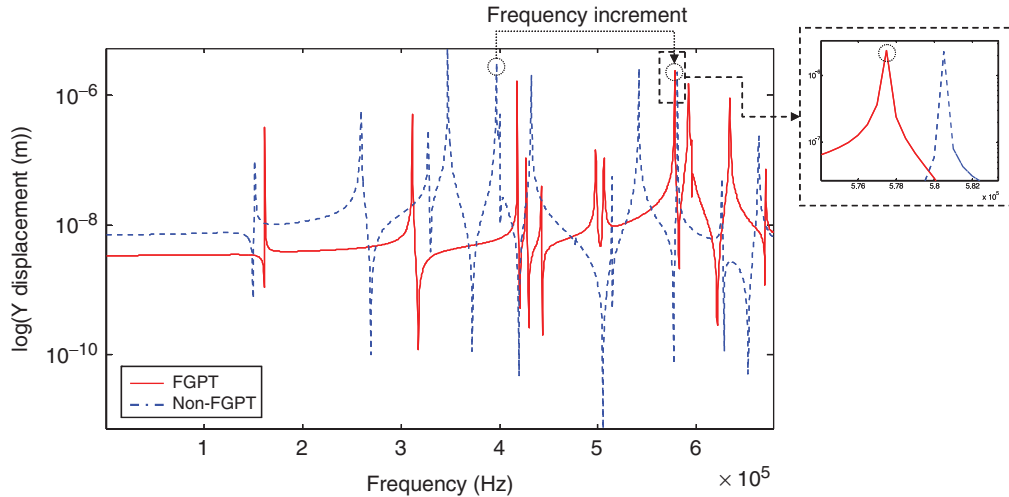


Figure 12. Axial mechanical FRF at the central point of the top surface for the FGPT of Figure 11(b).

presents a smoother gradation function than the non-projection related curve, see Figure 11(c).

Moreover, Figure 12 shows the axial mechanical FRF for the FGPT of Figure 11(b). It shows that the final eigenvalue corresponds to a piezoelectric mode with resonance frequency equal to 577.3 kHz. Hence, by using the technique here presented, a piezoelectric transducer with a resonance frequency at piston-like mode, increased by 46%, is obtained, in relation to the initial resonance frequency of the PZT-5A transducer (396.6 kHz).

An interesting problem consists of maximizing the first resonance frequency (ω_0) of an FGPT, aiming to reduce the time response t_{resp} ($t_{\text{resp}} = 1/\omega_0$); specifically, in quasi-static applications (Silva et al., 2000). In this example, the material types 1 and 2 are piezoelectric ceramic PZT-5A and PZT-2, respectively (see Table 1), which represent an FGPT type piezoelectric/piezoelectric. A mesh of 50×30 GFes is used and the first five eigenmodes are considered into the multi-objective function, considering $m = 5$ in Equation (13). All five weights are assumed equal to 1. Gradation along thickness direction is considered. Other important data for topology implementation are shown in Table 2.

The multi-objective convergence history, the final material distribution, and the axial mechanical FRF are shown in Figure 13. The projection technique leads to a smoother material distribution and quicker convergence than the non-projection case. When the projection technique is not used, the optimization algorithm tends to obtain a material gradation with high property gradients, almost close to a 0–1 design. The optimized gradation function represents an FGPT with PZT-2-rich region on the top and bottom surfaces, and also in the middle; while PZT-5A-rich region appears between middle-top region and middle-bottom region.

Figure 13(c) confirms the obtained result. The first resonance frequency is incremented from 151.6 to 270 kHz, which represents a frequency increment of 78% in relation to initial first resonance frequency obtained with PZT-5A material. This first resonance frequency of the topology optimized FGPT is higher even than the second resonance frequency of the initial PZT-5A transducer (259.2 kHz).

FGPT Design with Specified Resonance Frequencies

In this section, the objective function F_2 is maximized. The utilized design domain is shown in Figure 6, and it is discretized by using 50×30 finite elements. The material type 1 is represented for a PZT-5A piezoelectric ceramic, and the material type 2 is a non-piezoelectric material (epoxy resin), see Table 1. Material gradation along the thickness direction is assumed.

In this example, it is desired that the FGPT oscillates at piston-like mode (Figure 11(a)) with a prescribed resonance eigenvalue equal to $\lambda_{01} = 11.20 \times 10^{12} \text{ Hz}^2$ (or resonance frequency equal to 532.63 Hz). Figure 14 shows the convergence curves for the objective function, piston-like mode eigenvalue, and the desirable eigenmode position during the optimization process. It is observed that the objective function is minimized (Figure 14(a)); in other words, at each optimization step, the difference between the current and desirable eigenvalue is diminished. Also, the desirable eigenvalue is achieved; specifically, the reached eigenvalue is equal to $11.028 \times 10^{12} \text{ Hz}^2$ (Figure 14(b)), which differ from the desirable eigenvalue in less than 2%. In addition, the initial eigenvalue of the piston-like mode ($6.209 \times 10^{12} \text{ Hz}^2$) is increased by 78%. The piston-like mode switches its order vibration number during the optimization process (Figure 14(c)), which results in a converging non-smooth objective function.

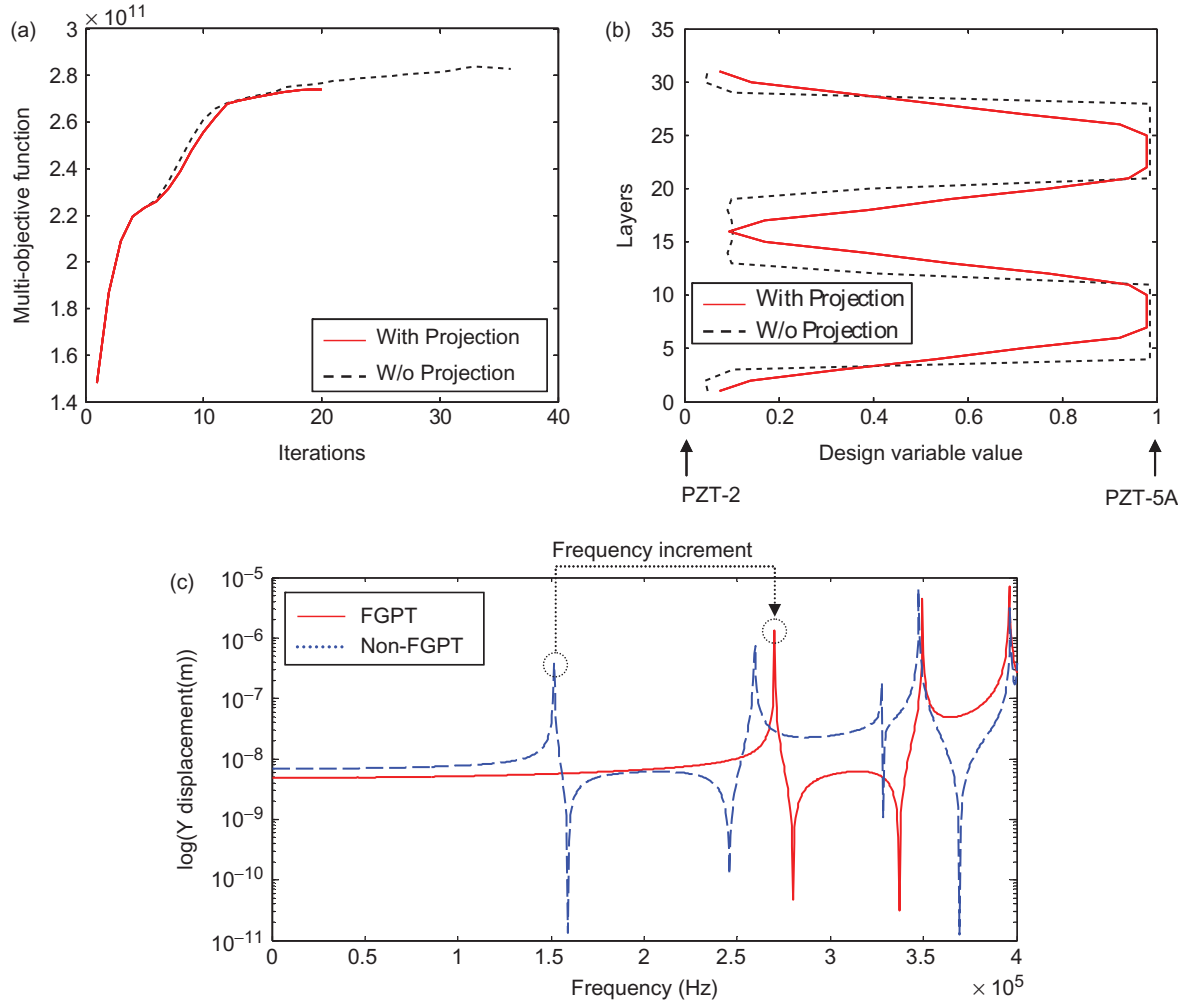


Figure 13. Maximizing first eigenvalue of FGPT: (a) multi-objective convergence history (F_1); (b) final gradation function; and (c) the axial mechanical FRF at the central point of the top surface.

On the other hand, Figure 15 shows a good correlation between initial user-defined eigenmode (piston-like mode shape, Figure 11(a)) and achieved eigenmode (Figure 15(a)); accordingly, the final mode shape is a thickness extensional mode. Also, Figure 15(b) exhibits the final material distribution function with and without projection technique. This solution depicts an FGPT with high piezoelectric properties in the middle (close to PZT-5A material) and non-piezoelectric properties on the top and bottom surfaces (close to polymer material). Again, the projection technique presents a smoother gradation function with relation to the non-projection curve.

Figure 16 shows the axial mechanical FRF for the topology optimized FGPT of Figure 15. The final eigenvalue of the piston-like mode corresponds to a piezoelectric mode with resonance frequency equal to 528.52 kHz, which is equivalent to achieved eigenvalue ($11.028 \times 10^{12} \text{ Hz}^2$). Thus, the difference between desirable (532.63 kHz) and achieved (528.52 kHz) resonance frequencies is less than 1%.

PMC Maximization of User-defined Mode Shapes

Here, the PMC of a user-defined vibration mode shape is maximized; by maximizing the objective function F_3 (Equation (15)). Figure 6 shows the design domain utilized to illustrate the method. A mesh of 50×30 finite elements is used, which represent an FGPT graded along thickness by using 31 layers. Material type 1 represents a PZT-5A ceramic and material type 2 represents a PZT-5H ceramic (Table 1). The reference thickness extensional mode (target mode) to be tracked along the iterative optimization process is shown in Figure 11(a) (deformed and non-deformed structure); in other words, the PMC of the piston-like mode (mode number 23) of Figure 8 should be maximized.

Figure 17 shows the final material distribution law (to maximize the PMC when the FGPT vibrates in the thickness extensional mode (piston-like mode)) and the vibration mode shapes when several r_{min} in Equation (21) are used. Specifically, Figure 17 depicts the gradation functions when non-projection technique and

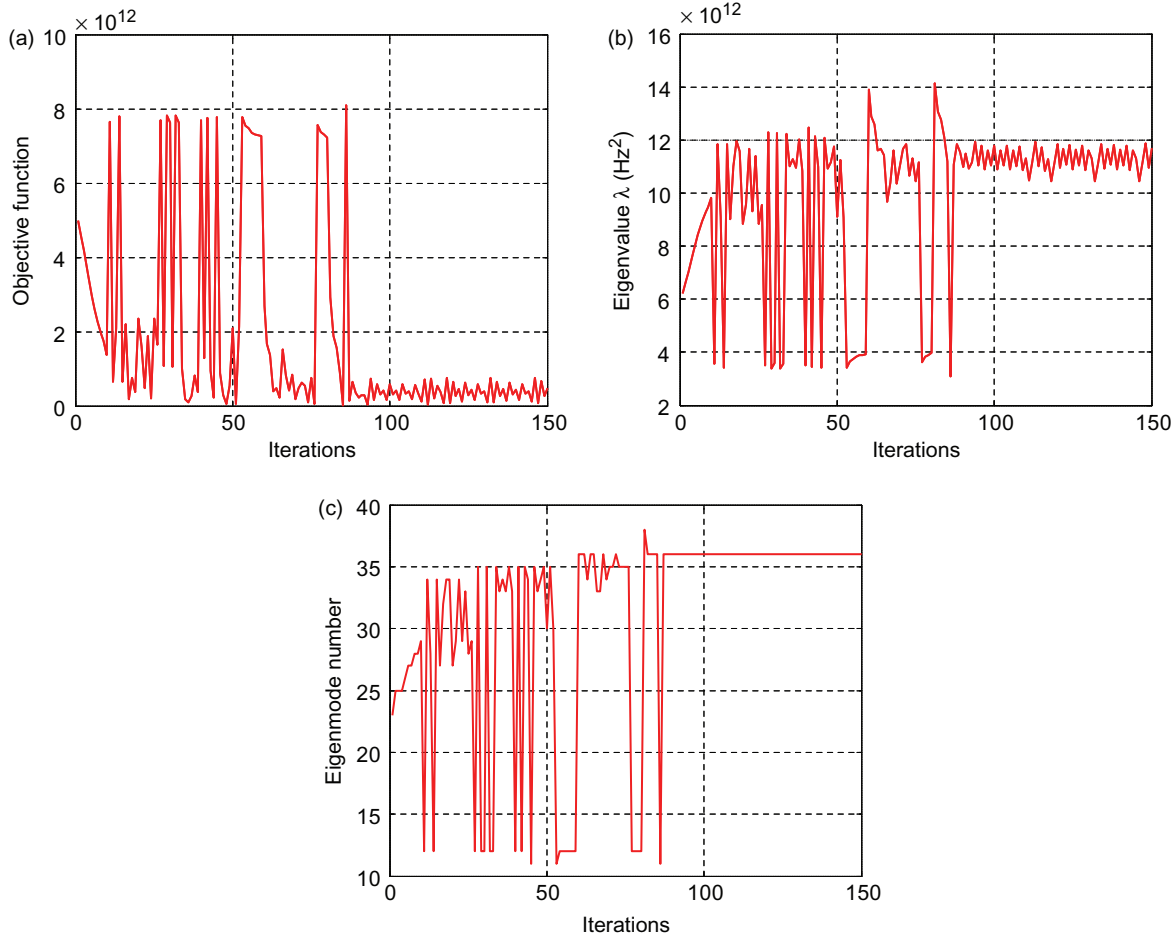


Figure 14. Convergence history curves for: (a) objective function (F_2), (b) eigenvalue, (c) mode position.

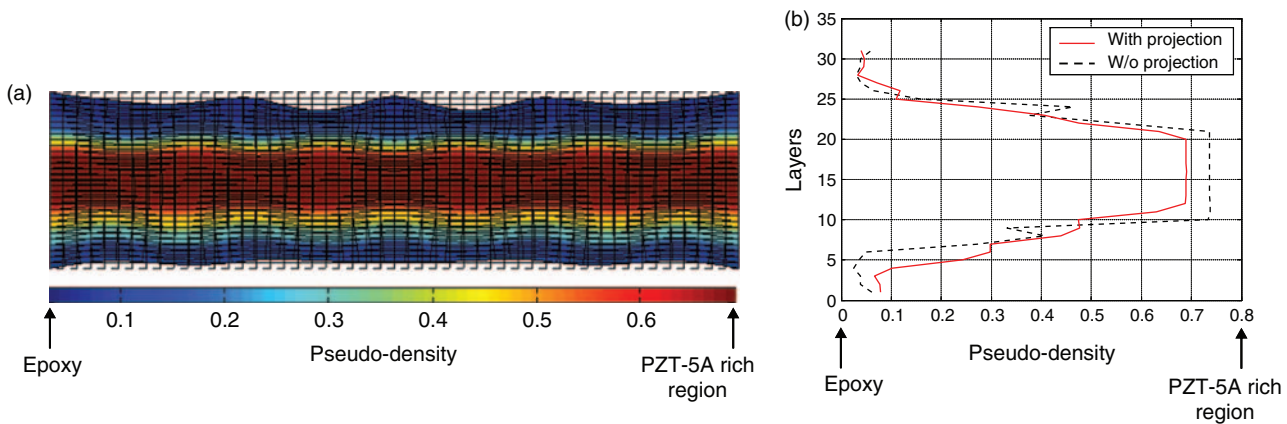


Figure 15. FGPT with specified resonance frequency (F_2 maximization): (a) final mode shape (dashed and solid line respectively depict non-deformed and deformed structure); (b) final material distribution function.

projection technique with r_{min} equal to 1.1; 1.8; 2.5 are utilized. When r_{min} is incremented, smoother gradation functions are obtained because the sub-domain S_i is incremented. On the other hand, Figure 17 shows that, in all simulated cases, the obtained mode shape is highly correlated with the initial mode shape (Figure 11(a)), and the final material distribution of the FGPT

represents a piezoelectric transducer with PZT-5A properties in the middle, but with PZT-5H-rich regions on the top and bottom surfaces. The result shows the advantage of using the FGM concept and TOM to design piezoelectric transducers with maximized PMC. Particularly, when an r_{min} equal to 1.8 is used, the material distribution increases the desirable PMC by 65%,

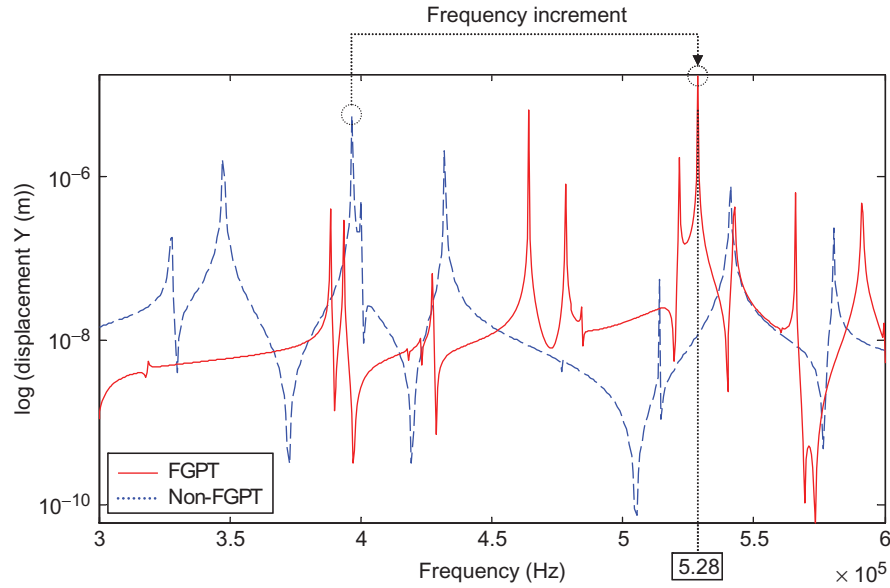


Figure 16. Axial mechanical FRF at the central point of the top surface of the FGPT of Figure 15, which refers to design with specific resonance frequency (F_2 maximization).

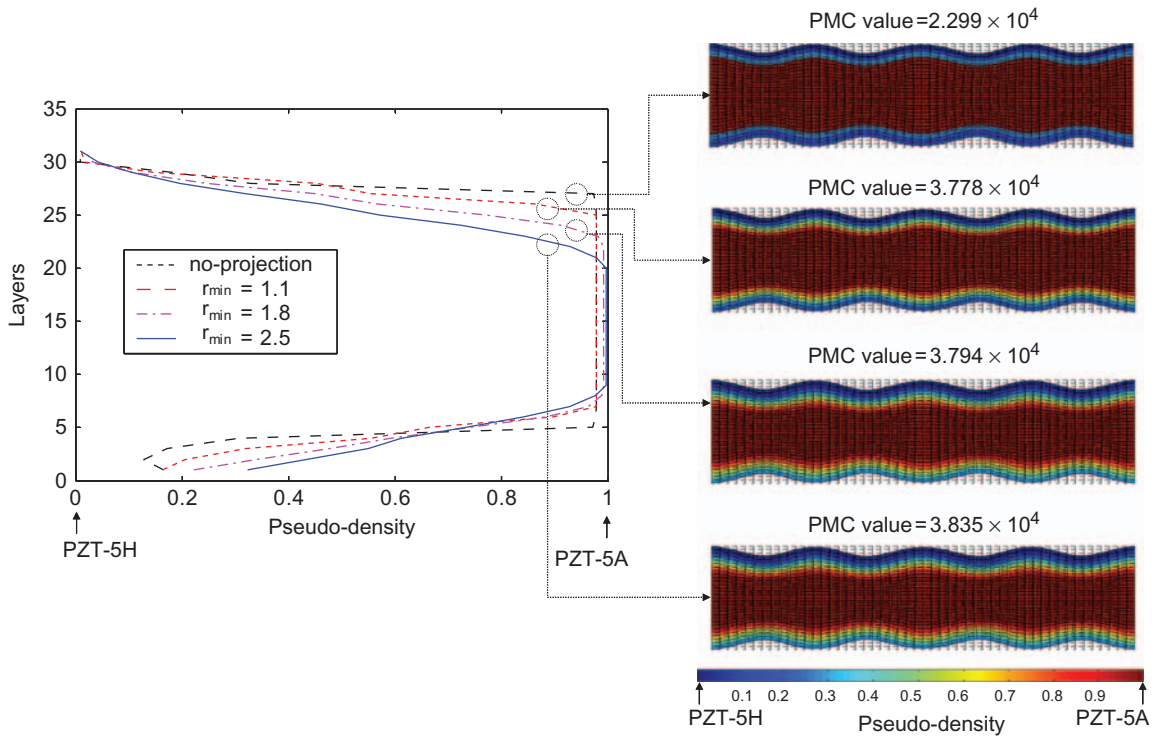


Figure 17. Final material distribution function and mode shapes when objective function F_3 is maximized and the length scale (r_{min}) is varied (Equation (21)).

i.e. 2.299×10^4 to 3.794×10^4 (Figure 18(a)). In other words, the strength of the piston-like mode is increased by 65% when a voltage is applied across the electrodes of the FGPT in relation to initial non-FGPT (with only PZT-5A properties). Figure 18(b) confirms that result and shows the PMC of the first fifty modes (including

elastic and piezoelectric modes) of the optimized FGPT. The PMC of the desirable piston-like mode (mode number 24) is the highest; thus, the optimized PMC is 880% and 441% higher than modes number 19 and 27 (adjacent modes), respectively. This dynamical behavior represents a uni-modal FGPT.

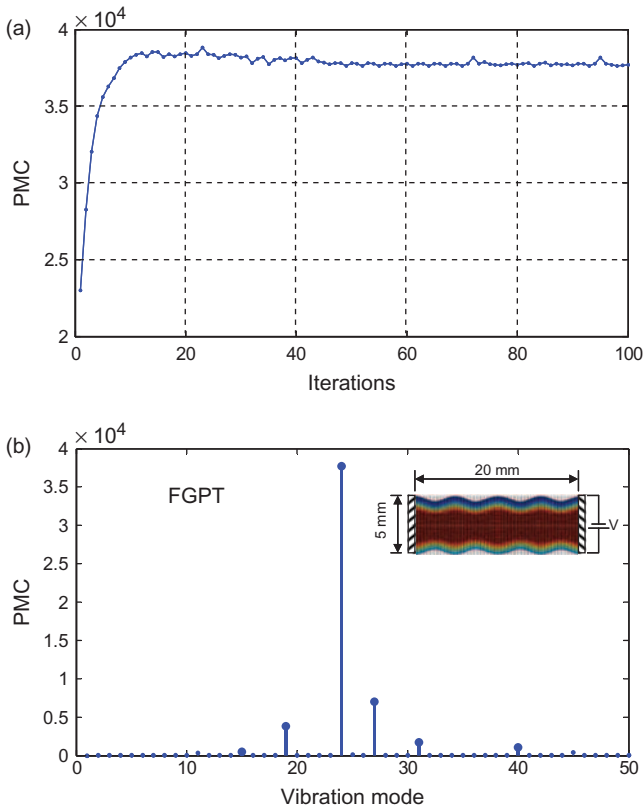


Figure 18. FGPT with maximized PMC (F_3 maximization) for length scale (r_{min}) equal to 1.8: (a) PMC convergence history; (b) first 50 normalized PMCs.

SUMMARY AND CONCLUSIONS

This article contributes to the optimal design of piezoelectric transducers based on multifunctional and smoothly graded hybrid material systems. The FGPT design is achieved by means of topology optimization, aiming to control/modify its dynamic performance. The FGPTs are designed using a continuum topology optimization algorithm based on: (i) GFE formulation to account for the material gradation inside each finite element; (ii) the CAMD approach to model a continuous design variable change; (iii) explicit gradient control via the projection technique; (iv) layer-like optimization approach for manufacturing requirements, where the design variables are considered equal at each interfacial layer, according to the gradation direction; in examples, along thickness direction; and (v) the MAC to track a user-defined mode shape. The TOM leads to the FGPT optimal gradation properties in terms of specific objective functions. These objective functions are: (i) to maximize eigenvalues of user-defined eigenmodes; (ii) to achieve desirable resonance frequencies and desirable vibration mode shapes; and (iii) to maximize PMC of specified eigenmodes.

The following conclusions can be drawn from this study:

1. The topology optimization method can be successfully applied as a systematic tool for designing FGPT; specifically, TOM can be applied to find optimal gradation function aiming at maximizing a proposed optimization goal.
2. The present technique is applicable to the design of both piezoelectric/piezoelectric and piezoelectric/non-piezoelectric FGPTs; in other words, TOM allows the simultaneous distribution of either two piezoelectric materials or a non-piezoelectric and a piezoelectric material in the design domain.
3. The projection technique helps to find smooth gradation function, which is desired for manufacturing purposes. In addition, the manufacturing of FGPT becomes possible by implementing the layer-like optimization; for instance, piezoelectric graded ceramics composed of green layers can be sintering by using the spark plasma sintering technique (Paulino et al., 2003).
4. The MAC arises as an adequate technique to follow desired mode shapes in FGPT. This is important for designing FGPT for wave generation applications; for instance, tracking piston-like mode as this mode is generally associated with high PMC.
5. The numerical examples demonstrate that TOM and FGM concept can increase the user-defined mode eigenvalue. Thus, FGPT with optimal graded properties along thickness direction may exhibit higher resonance frequency. In addition, FGPTs that vibrate at user-defined frequencies and user-defined mode shapes can be designed: high correlation is obtained between user-defined and final mode shape, and a small difference (less than 1% in the present study) is achieved at user-specified resonance frequency. Finally, a high increment (around 65% in the present study) is achieved when the PMC (electro-mechanical coupling) of the piston-like mode is maximized.

For future work, other objective functions can be considered on the optimization problem; such as designing narrowband and/or broadband FGPT. In addition, gradation along other directions can be considered besides thickness direction; for instance, gradation along longitudinal direction. Finally, the concept of hybrid materials should be further explored.

ACKNOWLEDGMENTS

The first author thanks FAPESP (São Paulo State Foundation Research Agency) for supporting him in his graduate studies through the fellowship No. 05/01762-5. The second author acknowledges the financial support from FAPESP research project (2006/57805-7) and from CNPq – National Council for

Research and Development, Brazil (304208/2006-0). The third author acknowledges FAPESP for providing him the visiting scientist award at the University of São Paulo (USP) through project number 2008/5070-0.

REFERENCES

- Almajid, A., Taya, M. and Hudnut, S. 2001. "Analysis of Out-of-plane Displacement and Stress Field in a Piezocomposite Plate with Functionally Graded Microstructure," *International Journal of Solids and Structures*, 38(19):3377–3391.
- Almeida, S.M.R., Paulino, G.H. and Silva, E.C.N. 2008. "A Simple and Effective Inverse Projection Scheme for Void Distribution Control in Topology Optimization," *Structural and Multidisciplinary Optimization*, DOI: 10.1007/s00158-008-0332-6 (in press).
- Banks-Sills, L., Eliasi, R. and Berlin, Y. 2002. "Modeling of Functionally Graded Materials in Dynamic Analyses," *Composites B*, 33(1):7–15.
- Bendsøe, M.P. and Sigmund, O. 2003. *Topology Optimization: Theory, Methods and Applications*, Springer, Berlin.
- Birman, V. and Byrd, W.L. 2007. "Modeling and Analysis of Functionally Graded Materials and Structures," *Applied Mechanics Review*, 60(5):195–216.
- Carbonari, R.C., Silva, E.C.N. and Paulino, G.H. 2009. "Multi-actuated Functionally Graded Piezoelectric Micro-tools Design: A Multiphysics Topology Optimization Approach," *International Journal for Numerical Methods in Engineering*, 77(3):301–336.
- Carbonari, R.C., Silva, E.C.N. and Paulino, G.H. 2007. "Topology Optimization Design of Functionally Graded Bimorph-type Piezoelectric Actuators," *Smart Materials and Structures*, 16(6):2607–2620.
- Carbonari, R.C., Silva, E.C.N. and Nishiwaki, S. 2005. "Design of Piezoelectric Multi-actuated Microtools Using Topology Optimization," *Smart Materials and Structures*, 14(6):1431–1447.
- Carrillo-Heian, E.M., Carpenter, D., Paulino, G.H., Gibel, J.C. and Munir, Z.A. 2001. "Dense Layered Molybdenum Disilicide-Silicon Carbide Functionally Graded Composites Formed by Field-activated Synthesis," *Journal of the American Ceramic Society*, 84(5):962–968.
- Chakraborty, A., Gopalakrishnan, S. and Kausel, E. 2005. "Wave Propagation Analysis in Inhomogeneous Piezo-composite Layer by The Thin Layer Method," *International Journal for Numerical Methods in Engineering*, 64(5):567–598.
- Diaz, A. and Kikuchi, N. 1992. "Solution to Shape and Topology Eigenvalue Optimization Problems Using a Homogenization Method," *International Journal for Numerical Methods in Engineering*, 35(7):1487–1502.
- Ewins, D.J. 1988. *Modal Testing: Theory and Practice*, Research Studies Press, England.
- Guest, J.M., Prevost, J.H. and Belytschko, T. 2004. "Achieving Minimum Length Scale in Topology Optimization Using Nodal Design Variables and Projection Functions," *International Journal for Numerical Methods in Engineering*, 61(2):238–254.
- Guo, H., Cannata, J., Zhou, Q. and Shung, K. 2005. "Design and Fabrication of Broadband Graded Ultrasonic Transducers with Rectangular Kerfs," *IEEE Transaction on Ultrasonics, Ferroelectrics, and Frequency Control*, 52(11):2096–2102.
- Guo, N. and Cawley, P. 1992. "Measurement and Prediction of the Frequency Spectrum of Piezoelectric Disks by Modal Analysis," *Journal of the Acoustical Society of America*, 92(6):3379–3388.
- Ha, H. and Cho, S. 2006. "Design Sensitivity Analysis and Topology Optimization of Eigenvalue Problems for Piezoelectric Resonators," *Smart Materials and Structures*, 15(6):1513–1524.
- Haftka, R.T., Gürdal, Z. and Kamat, M.P. 1990. *Elements of Structural Optimization*, Kluwer Academic Publishers, Dordrecht.
- Haue, T., Kouvatov, A., Steinhausen, R., Seifert, W., Beige, H., Langhammer, H.T. and Abicht, H. 2000. "Bending Behavior of Functionally Graded Materials," *Ferroelectrics*, 238(1):195–202.
- Kim, T.S. and Kim, Y.Y. 2000. "MAC-based Mode-tracking in Structural Topology Optimization," *Computers and Structures*, 74(3):375–383.
- Kim, J.K. and Paulino, G.H. 2002. "Isoparametric Graded Finite Elements for Nonhomogeneous Isotropic and Orthotropic Materials," *ASME Journal of Applied Mechanics*, 69(4):502–514.
- Kino, G. 2000. *Acoustic Waves: Devices, Imaging, and Analog Signal Processing*, Corrected edn, Prentice-Hall, Inc. New Jersey.
- Kögl, M. and Silva, E.C.N. 2005. "Topology Optimization of Smart Structures: Design of Piezoelectric Plate and Shell Actuators," *Smart Materials and Structures*, 14(2):387–399.
- Kruusing, A. 2000. "Analysis and Optimization of Loaded Cantilever Beam Microactuators," *Smart Materials and Structures*, 9(2):186–196.
- Le, C.H. 2006. *Achieving Minimum Scale and Design Constraints in Topology Optimization: A New Approach*, University of Illinois at Urbana-Champaign, Master thesis.
- Lee, H.-J. 2005. "Layerwise Laminated Analysis of Functionally Graded Piezoelectric Bimorph Beams," *Journal of Intelligent Material Systems and Structures*, 16(4):365–371.
- Lerch, R. 1990. "Simulation of Piezoelectric Devices by Two- and Three-dimensional Finite Elements," *IEEE Transactions on Ultrasonics, Ferroelectrics, and Frequency Control*, 37(2):233–247.
- Ma, Z.D., Kikuchi, N. and Cheng, H.C. 1995. "Topology Design for Vibration Structures," *Computer Methods in Applied Mechanics and Engineering*, 121(1–4):259–280.
- Matsui, K. and Terada, K. 2004. "Continuous Approximation of Material Distribution for Topology Optimization," *International Journal for Numerical Methods in Engineering*, 59(14):1925–1944.
- Miyamoto, Y., Kaysser, W.A., Rabin, B.H., Kawasaki, A. and Ford, R.G. 1999. *Functionally Graded Materials: Design, Processing and Applications*, Kluwer Academic Publishers, Dordrecht.
- Naillon, M., Coursant, R.H. and Besnier, F. 1983. "Analysis of Piezoelectric Structures by a Finite Element Method," *Acta Electronica*, 25(4):341–362.
- Paulino, G.H., Jin, Z.H. and Dodds, R.H. 2003. "Failure of Functionally Graded Materials," In: Karihaloo, B. and Knauss, W.G. (eds), *Comprehensive Structural Integrity*, Vol. 2, Chap. 13, pp. 607–644, Elsevier Science, New York.
- Qui, J., Tani, J., Ueno, T., Morita, T., Takahashi, H. and Du, H. 2003. "Fabrication and High Durability of Functionally Graded Piezoelectric Bending Actuators," *Smart Materials and Structures*, 12(1):115–121.
- Rahmatalla, S.F. and Swan, C.C. 2004. "A Q4/Q4 Continuum Structural Topology Optimization Implementation," *Structural Multidisciplinary Optimization*, 27(1–2):130–135.
- Rubio, W.M., Buiochi, F., Adamowski, J.C. and Silva, E.C.N. 2009. "Modelling of Functionally Graded Piezoelectric Ultrasonic Transducers," *Ultrasonics*, 49(4–5):484–494.
- Santare, M.H., Thamburaj, P. and Gazonas, G.A. 2003. "The Use of Graded Finite Elements in the Study of Elastic Wave Propagation in Continuously Nonhomogeneous Materials," *International Journal of Solids and Structures*, 40(21):5621–5634.
- Santare, M.H. and Lambros, J. 2000. "Use of Graded Finite Elements to Model the Behavior of Nonhomogeneous Materials," *Journal of Applied Mechanics*, 67(4):819–822.
- Shindo, Y., Narita, F. and Nakagawa, J. 2009. "Dynamic Electromechanical Response and Self-Sensing of Functionally Graded Piezoelectric Cantilever Transducers," *Journal of Intelligent Material Systems and Structures*, 20(1):119–126.
- Sigmund, O. and Torquato, S. 1999. "Design of Smart Composite Materials Using Topology Optimization," *Smart Materials and Structures*, 8(3):365–379.
- Silva, E.C.N., Carbonari, R.C. and Paulino, G.H. 2007. "On Graded Elements for Multiphysics Applications," *Smart Materials and Structures*, 16(6):2408–2428.
- Silva, E.C.N., Nishiwaki, S. and Kikuchi, N. 2000. "Topology Optimization Design of Flexensional Actuators," *IEEE Transactions on Ultrasonics, Ferroelectrics, and Frequency Control*, 47(3):657–671.

- Silva, E.C.N. and Kikuchi, N. 1999. "Design of Piezoelectric Transducers Using Topology Optimization," *Smart Materials and Structures*, 8(3):350–364.
- Silva, E.C.N., Fonseca, O.J.S., Montero de Espinosa, F., Crumm, A.T., Brady, G.A., Halloran, J.W. and Kikuchi, N. 1999. "Design of Piezocomposite Materials and Piezoelectric Transducers Using Topology Optimization – Part I," *Archives of Computational Methods in Engineering*, 6(2):117–182.
- Soto, C.A. and Diaz, A.R. 1993. "Layout of Plate Structures for Improved Dynamic Response Using a Homogenization Method," Proceedings of the 1993 ASME DETC, pp. 667–674, Advances in Design Automation, Albuquerque, NM.
- Steinhausen, R., Kouvatov, A., Beige, H., Langhammer, H.T. and Abicht, H.-P. 2004. "Poling and Bending Behavior of Piezoelectric Multilayers Based on Ba(Ti,Sn)O₃ Ceramics," *Journal of the European Ceramic Society*, 24(6):1677–1680.
- Sutter, R.T., Camarda, J.C., Walsh, L.J. and Adelman, M.H. 1988. "Comparison of Several Methods for Calculating Vibration Mode Shape Derivates," *AIAA Journal*, 26(12):1506–1511.
- Taya, M., Almajid, A.A., Dunn, M. and Takahashi, H. 2003. "Design of Bimorph Piezocomposite Actuators with Functionally Graded Microstructure," *Sensors and Actuators A-Physical*, 107(3):248–260.
- Wang, B.P. 1990. "Improved Approximate Methods for Computing Eigenvector Derivates in Structural Dynamics," *AIAA Journal*, 29(6):1018–1020.
- Wang, B.L. and Noda, N. 2001. "Design of a Smart Functionally Graded Thermopiezoelectric Composite Structure," *Smart Material Structure*, 10(2):189–193.
- Yang, J. and Xiang, H.J. 2007. "Thermo-electro-mechanical Characteristics of Functionally Graded Piezoelectric Actuators," *Smart Materials and Structures*, 16(3):784–797.
- Yong, Y.K. and Cho, Y. 1996. "Numerical Algorithms for Solutions of Large Eigenvalue Problems in Piezoelectric Resonators," *International Journal for Numerical Methods in Engineering*, 39(6):909–922.
- Zhang, Z. and Paulino, G.H. 2007. "Wave Propagation and Dynamic Analysis of Smoothly Graded Heterogeneous Continua Using Graded Finite Elements," *International Journal of Solids and Structures*, 44(11):3601–3626.
- Zhong, Z. and Yu, T. 2006. "Vibration of a Simply Supported Functionally Graded Piezoelectric Rectangular Plate," *Smart materials and Structures*, 15(5):1404–1412.

APPENDIX: LIST OF SYMBOLS

Latin Symbols

- x, y = Cartesian coordinates
- r = subscript indicating resonance condition
- a = subscript indicating antiresonance condition
- k = subscript indicating the number of the vibration mode
- e = indicates finite element
- o = subscript denoting the electrical potential d.o.f of the non-electrode nodes
- p = subscript denoting the electrical potential d.o.f of the ungrounded electrode node
- g = subscript denoting the electrical potential d.o.f of the grounded electrode nodes
- w_k = weight coefficients for mode k
- m = number of modes considered in the multi-objective function
- n = user-defined power at objective functions
- n_d = number of nodes per finite element
- r_{min} = user-defined radius in the projection technique

- r_{ij} = radius between nodes i and j
- A = piezoelectric modal constant
- E = material properties for material type 1 or 2
- E^H = homogenized material properties
- F = represents objective function
- N = shape function per node
- N_{des} = number of nodes of discretized domain
- N_{type1} = number of nodes with material type 1
- S_i = sub-domain corresponds to a circle with its center located at the node i
- T = indicates transpose
- V_i = material volume at node i
- V^* = constraint for design variables related to material type 1
- W = weight function in the projection technique
- \mathbf{T} = second-order stress tensor
- \mathbf{D} = electric displacement vector
- \mathbf{C}^E = elasticity property tensor, (elastic stiffness at constant electric field)
- \mathbf{e} = piezoelectric property tensor
- \mathbf{r} = unit vector in the Cartesian coordinate system
- \mathbf{u} = displacement vector
- \mathbf{U} = nodal displacement vector
- \mathbf{F} = nodal mechanical force vector
- \mathbf{Q} = nodal electric charge vector
- \mathbf{M}_{uu} = mass matrix
- \mathbf{K}_{uu} = 'stiffness' elastic matrix
- $\mathbf{K}_{u\phi}$ = 'stiffness' piezoelectric matrix
- $\mathbf{K}_{\phi\phi}$ = 'stiffness' dielectric matrix
- \mathbf{N}_u = shape functions for the displacements
- \mathbf{B}_u = strain–displacement matrix
- \mathbf{B}_ϕ = voltage–gradient matrix
- \mathbf{W}_F = equivalent nodal force vector
- \mathbf{I}_p = vector of the ungrounded electrode nodes

Greek Symbols

- λ = eigenvalue
- λ_0 = user-specified eigenvalue
- ρ = density of material
- ω = circular natural frequency
- ρ_{TOM} = design variable or pseudo-density.
- ρ_{TOM}^e = pseudo-density at finite element e
- ρ_{TOM}^p = nodal pseudo-density
- $\rho_{TOM_j}^p$ = pseudo-density located at node j
- ρ_{TOM}^n = nodal design variable
- $\rho_{TOM_i}^n$ = design variable located at node i
- Ω = bi-dimensional design domain
- Ω_s = design domain with material type 1
- ϕ = nodal electric potential vector
- ϵ^S = dielectric property tensor, (dielectric susceptibility at constant strain)
- Ψ = eigemode vector
- Ψ_u = mechanical component of eigenmode vector
- Ψ_ϕ = electrical component of eigenmode vector
- Ψ_{ref} = user-defined or target mode shape
- Ψ_c = current mode shape at each iteration of the optimization process